SYNTHESIS OF NEW MATERIALS

Francesco Giacalone,[a*] Michelangelo Gruttadauria,[a]

[a] *Università degli Studi di Palermo, Dipartimento di Scienze e Tecnologie Biologiche, Chimiche e Farmaceutiche (STEBICEF), Via delle Scienze s/n, Parco d'Orleans - Edificio 17, 90128 Palermo*
e-mail: francesco.giacalone@unipa.it

1. INTRODUCTION

Nowadays the Chemistry of Materials is a well-known but yet expanding field. The use of improved materials enables scientists and engineers to design new processes and better final products. Hence, the Society is the recipient of such sophisticated new materials able to save lives, produce green energy and expand human horizons. In the twentyfirst century chemists are called to develop or to improve a new generation of materials in order reshape our world and solve some of the planet's most pressing problems.

Materials composed of both inorganic and organic entities are called hybrid materials. They combine, to some extent, the properties of both constituents in a unique material and represent an old challenge since the beginning of the industrial era. The general idea behind these materials is similar to that of composites, where two or more materials that differ in form and chemical composition are combined. While macroscopic constituents with defined phase boundaries are used for composite materials, molecular building blocks of different composition (inorganic and organic/organometallic/biological) are instead combined in hybrid materials. The combination of different building blocks allows the generation of materials with new properties or combinations of properties not accessible otherwise. The research on hybrid materials is interdisciplinary because different synthetic methodologies are involved, as well as many different physical characterization techniques are used. The success of the hybrid material research is increasingly relying upon the collective efforts from various disciplines. Nevertheless, chemists are playing a significant role since the synthesis of these advanced materials is certainly about how to assemble atoms or molecules into nanostructures of desired coordination environment, sizes, and shapes.

The aim of the present chapter is not to cover the whole spectrum of possible materials and synthetic techniques, which would be limitless, but just present highlights on some outstanding hybrid functional material reported during the year 2012. Emphasis will be put on the synthetic strategies followed to prepare and to characterize them, as well as on their applications.

2. HYBRID ORGANIC-INORGANIC MATERIALS

To date a huge number of functional hybrid materials have been reported in the literature which find application in many different fields such as catalysis, sensing, separation, photovoltaics, bioengineering, among others. Although the preparation of these materials often need specific protocols or particular analytical and spectroscopical techniques for their determination, all of them require a modular approach to be followed. Indeed, each material before to be used for practical application needs first to be projected, then prepared by following the proper synthetic strategies and subsequently characterized by means of the appropriate techniques (Fig. 1).

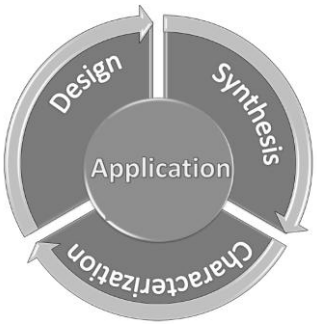

Fig. 1. Modular approach toward a functional hybrid material.

During the design of hybrid materials inorganic and organic parts are chosen as well as the functionalities which have to link them. Then the proper synthetic protocols are applied in order to prepare all the synthons and, finally, the hybrid is assembled both through the formation of covalent bonds or by supramolecular interactions or simply through entrapping the inorganic part within the organic one. Hence, the analytical and spectroscopical characterization take place in order to undoubtedly establish the right composition and functionalities present in the new hybrid. The last and hard part of the work is to demonstrate that the obtained material is really able to carry out the work it was projected for. As stated before, due to the high number of different materials and applications present in the literature herein a comprehensive treatise is out of the scope of the present survey. Nevertheless, an overview of selected outstanding examples showing different methodology to form hybrid materials and their final application will be herein reported. We will focus our attention mainly in few types of hybrid assemblies: polyoxometalates, metal-organic frameworks, modified silicas, magnetic nanoparticles and carbon nanoforms.

2.1 POLYOXOMETALATES

Polyoxometalates (POMs) are a big family of early-transition-metal oxygen-anion nano-sized clusters with a completely inorganic, metal oxide-like structure, stable to oxidation. This class of compounds is raising huge interest due to a unique combination of properties, such as good thermal and hydrolytic stability, a wide variety of structures and compositions, tunable acidity, redox potentials and solubility, etc. POMs maybe meant as discrete and soluble fragments of extended metal oxide lattices (Fig. 2). In addition, POMs can be easily investigated at the atomic level, both structurally and mechanistically, which makes them good objects for studying structure-activity relationships and mechanisms of catalysis.

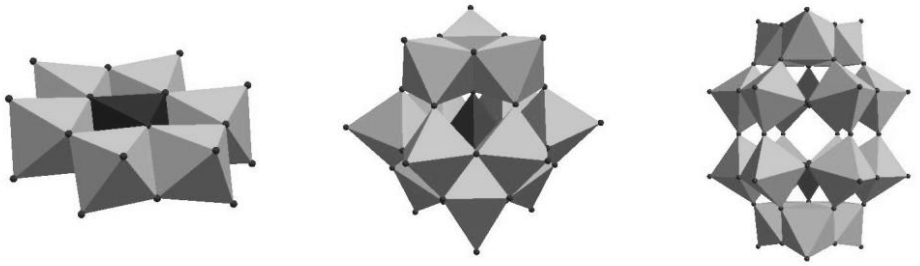

(a) (b) (c)

Fig. 2. General examples of POM: (a) Anderson structure, $XM_6O_{24}^{n-}$; (b) Keggin structure, $XM_{12}O_{40}^{n-}$; (c) Dawson structure, $X_2M_{18}O_{62}^{n-}$.

One of the possible manners to incorporate POMs into hybrids is to exploit the ionic self-assembly (ISA). In fact POMs as polyanions are surrounded by several cations in order to keep electroneutrality, and these positive charges can be easily exchanged by polycationic species. POM **1** shows the peculiarity to undergo a quick and chemically reversible 8-electron reduction process without decomposition but its water solubility impede the recovery from aqueous solutions. To overcome this drawback, the ISA approach has been followed to incorporate the macrocyclic $[H_7P_8W_{48}O_{184}]^{33-}$ POM **1** into imidazolium-based poly ionic liquids (PILs) **4a,b** affording water insoluble visible light photosensitive catalysts.[1] The synthesis of PILs is straightforward and can be achieved in two steps (Scheme 1). First 4-chloromethylstyrene is reacted with the *N*-substituted imidazole and finally the corresponding monomers are polymerized with the help of a radical initiator (AIBN). The assemblies were precipitated by mixing PILs and 1 in HCl 1 M. The so formed hybrid were characterized by means of several techniques. TGA showed an increased stability of the polymer backbone in the assemble, whilst FT IR analysis presented the vibrations characteristic of both PILs and POM. Interestingly, in diffuse reflectance UV-vis-NIR spectroscopy (DRS) not only the whole spectra was largely red shifted

compared to those of the PILs or POM alone, but also presented an additional absorption band throughout all the visible and NIR regions which was associated with an electron transfer from PIL to **1**, as confirmed by spectroelectrochemistry. Moreover such electron transfer increases was proven to be light driven and the photosensitivity of the hybrids was marked mainly in samples containing **1** as POM.

What is important here is that, the single components are not photosensitive but is their combination into hybrid materials which affords this new property.

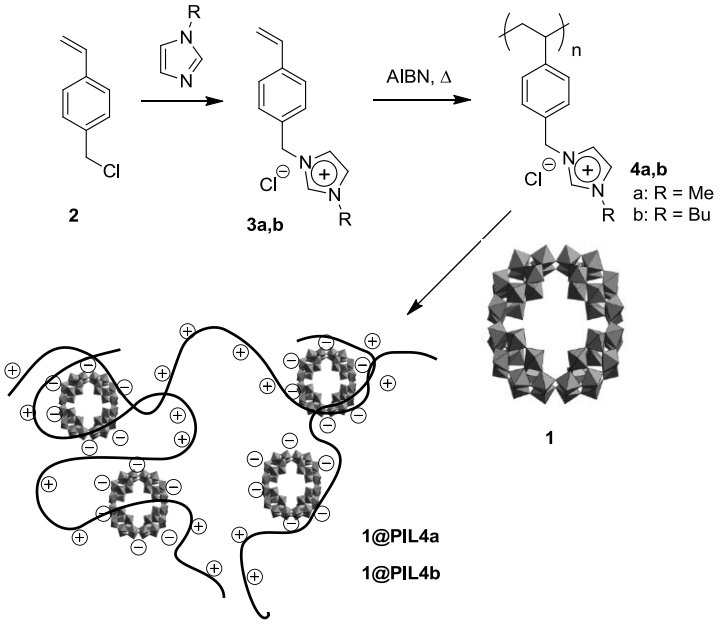

Scheme 1. Synthesis of POM-poly Ionic liquids hybrids

The remarkable electrochemical properties of **1** along with the heterogeneous nature of the POM-PIL hybrids and their photosensitivity prompted to exploit all these characteristics in photocatalysis under visible or solar light. In particular, hybrids were applied in the photodegradation of acid orange 7 (AO7), a highly toxic azo dye resistant to biodegradation and UV-vis photodegradation, in aqueous media with oxygen as an eco-friendly oxidant. Upon photolysis of **1@PIL4a** dispersions in oxygenated solutions of AO7, the intensities of all the AO7 absorbance peaks decrease with increasing the irradiation time (Fig 3a). The decrease of AO7 concentration in the presence of 1, PIL 4a, **1@IL4a** and **1@PIL4a** in function of irradiation time are reported in Fig 3b. Photodegradation efficiencies of **1** and PIL **4a** are very weak in comparison to those of **1@IL4a** and **1@PIL4a** being this latter material able to promote the total destruction of AO7 in just 60 min. This finding makes these kind of novel hybrid heterogeneous material suitable for environmental purposes.

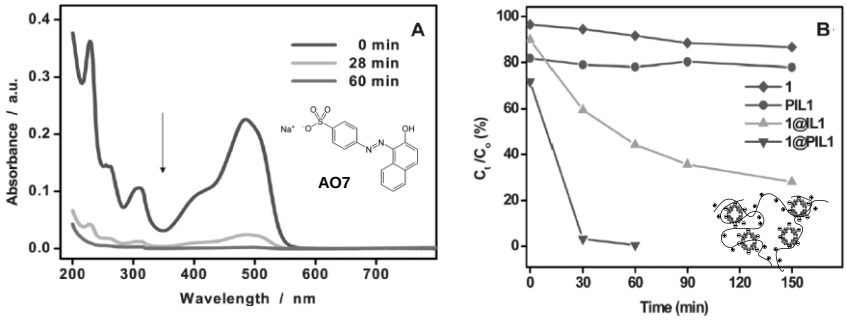

Fig. 3. a) UV-vis absorption spectral changes observed for an irradiated AO7 oxygenated solution as a function of the time in the presence of **1@PIL4a**; b) Time profiles of the photodegradation in pH 1 medium under visible light irradiation of AO7.

The versatility of POM-based materials stems from the fact that they can accommodate many different metals atoms in their framework exhibiting thus a variety of functional properties. In this light, Gadolinium-based paramagnetic POMs can be used as bio-imaging contrast agents (CAs) in magnetic resonance imaging (MRI), instead of Gd^{III}-based chelate complexes. However, in the physiological environment polyanions can bind strongly the positively charged biological molecules, which can be detrimental for the efficiency and biocompatibility of POMs as CAs in clinical use. A way to overcome these problems is the ISA approach employing the designed amphiphilic surfactant-like molecule endowed with a quaternary ammonium head group $EO_{12}BphC_{10}NC_{12}$ **9** (Scheme 2).[2]

The synthesis of **9** is rather easy requiring four high yielding synthetic steps involving three nucleophilic substitutions, starting from an oligoethylene glycol.

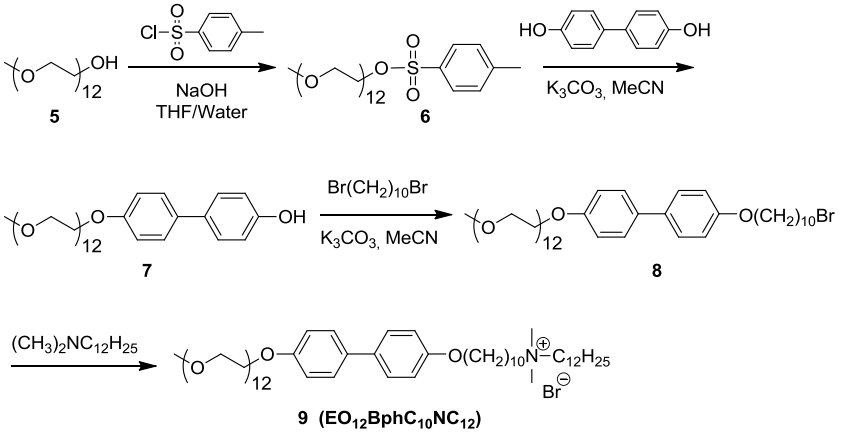

Scheme 2. Synthesis of surfactant-like molecule **9**.

Once prepared, a solution of **9** in chloroform was mixed with and aqueous solutions of $K_{13}[Gd(\beta_2\text{-}SiW_{11}O_{39})_2]\cdot 27H_2O$ forming cation-encapsulated gadolinium-substituted POM (OCEP-Gd) hybrids through electrostatic interactions which phase-separated and rearranged into a monolayer vesicle in aqueous solution (Fig. 4a). The so-obtained hybrid has been characterized by means of FT-IR, TGA and dynamic light scattering (DLS). This latter indicates that OCEP-Gd is in an aggregated state in water when the concentration is above critical aggregation concentration (7×10^{-4} mM) with a hydrodynamic radius of approximately 160 nm, which was further confirmed by Cryo-TEM and SEM analyses (Fig 4b-c). Finally, X-ray diffraction (XRD) measurement of OCEP-Gd aggregates showed multi-level diffractions indicating the ordered aggregation and vesicular structure of the assembly (Fig. 4d). The lamellar spacing estimated from the XRD data is 6.8 nm, close to the ideal height of an OCEP-Gd single layer. Finally, DLS studies also revealed that OCEP-Gd aggregates have good stability in physiological medium. This finding coupled with relaxation rate studies, which demonstrated the ability OCEP-Gd to accelerate the water-proton relaxation, clearly indicate the possible use of OCEP-Gd as contrast agents for MRI.

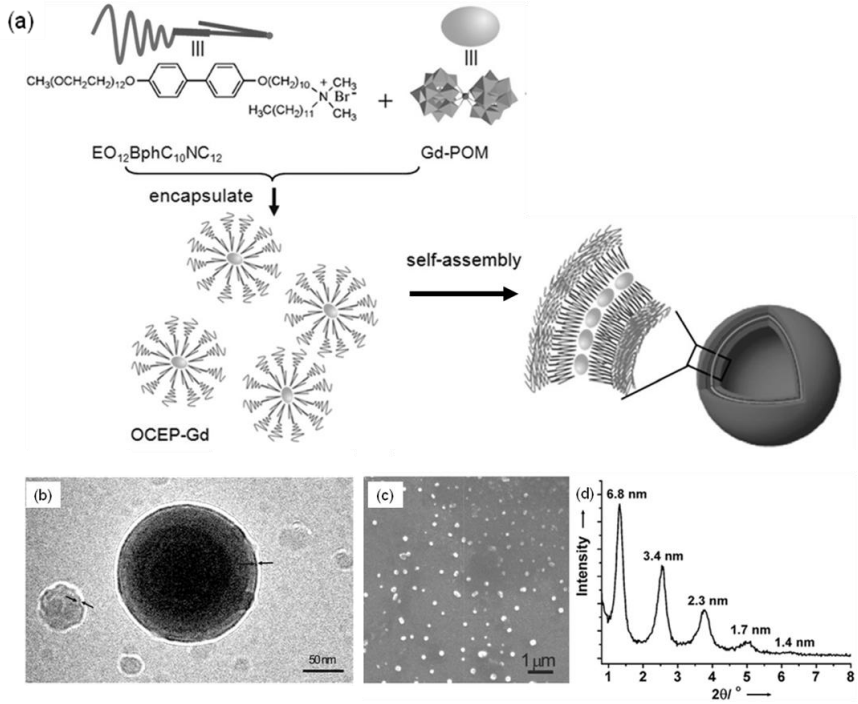

Fig. 4. a) Drawing for the preparation and aggregation of OCEP-Gd; b) Cryo-TEM and c) SEM images of OCEP-Gd aggregates in water; d) XRD pattern of OCEP-Gd aggregates.

On the other hand, when a catalytically activated sandwich-type polyoxometalate such as $Na_{12}[WZn_3(H_2O)_2(ZnW_9O_{34})_2]$ is encapsulated through electrostatic interactions by a chiral amphiphilic cation with two stereocenters, the so-formed chiral organic cation-encapsulated POM complex (COEP) may transfer chiral information during catalyzed organic processes.[3] The encapsulation process proceeds quickly by mixing at room temperature (+)-bis[(*R*)-1-phenylethyl]amine hydrochloride (*R*-BPEA) and the POM for 2 hours (Scheme 3). Elementary analysis and TGA confirmed that formed precipitate COEP-1*R* has 12 units of R-BPEA for each POM moiety being all the counterions of POM replaced by organic cations. IR analysis showed the POM characteristic vibrational bands whilst UV confirmed the absorption of the phenyl rings. Transferring of chirality has been confirmed by circular dichroism spectroscopy (CD) which showed for COEP-1*R* and COEP-1*S* mirror symmetric CD spectra. Interestingly, hybrid complexes showed self-assembly behavior under the reaction conditions (chloroform/H_2O_2 30% v/v in water) and DLS study revealed the presence of stable assemblies with 106 nm hydrodynamic diameter, further confirmed by TEM and SEM measurements. The non ordered structure of the yet tight packed assembly was finally proven by X-ray diffraction.

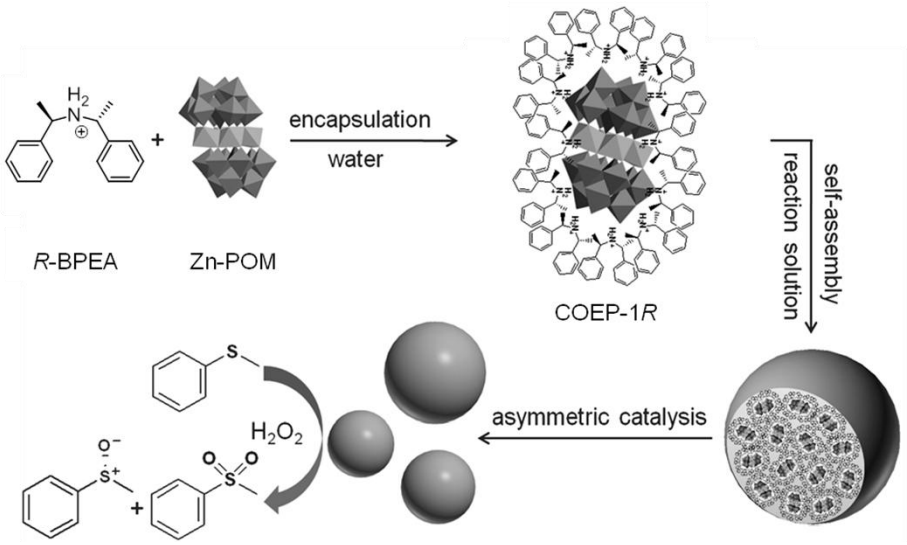

Scheme 3. Preparation procedure of COEP-1*R* assemblies and their asymmetric catalytic oxidation for methyl phenyl sulfide with H_2O_2 (30%)

The observed self-assemblies showed to be favorable for improving the chiral microenvironment around the POMs. The tight packing fixes chiral groups stiffly and increases the coverage density of the stereocenter on the POM surface in the assemblies. In fact, the catalytic oxidation of methyl phenyl sulfide with H_2O_2 promoted by 0.1 mol% of COEP-1*R* gave no enantiomeric excess in the polar

acetonitrile (in which assemblies are not formed) whist furnished a 16% ee in $CHCl_3$. However, increasing the amount of H_2O_2 results in increased ee (40%) but also in the overoxidation of the sulfoxide to sulfone, which reaches the 95% of yield extending the reaction time leaving the (*R*)-sulfoxide with a 72% ee. This behavior has been rationalized through kinetic studies which revealed that the direct oxidation of sulfide to solfoxide produce the (*R*) enantiomer with 20% ee but, after 3h the main process a kind of kinetic resolution in which the (*S*)-sulfoxide is efficiently transformed into the sulfone, leaving the (*R*)-sulfoxide in 70% ee. Although the enantioselectivity was not elevated this example offers a strategically universal protocol for the direct and efficient construction of more selective and robust supramolecular asymmetric catalysts based on POMs, which is important for potential applications in asymmetric synthesis.

Another manner to include POMs into hybrid materials rely on the covalent chemical functionalization of lacunary POMs precursors. These latter have in their surface coordination defects obtained by removing one or more metal-oxo polyhedron from the parent POM structures and usually present remarkable reactivity especially toward electrophiles such as organophosphonic acids, organosilanes, and organotin species, among others. Recently, three different lacunary POMs, namely $K_8[\alpha\text{-}SiW_{11}O_{39}]$, $K_8[\gamma\text{-}SiW_{10}O_{36}]$, and $Na_{10}[\alpha\text{-}SiW_9O_{34}]$ have been post-functionalized under phase-transfer conditions in the presence of TBA cations in order to accede to hybrid polymerizable POMs **10-12** (Scheme 4a).[4] The reactions of silylation smoothly proceeded with 50-83% yields, and these new molecular hybrids were fully characterized by means of ^{183}W NMR, ^{29}Si NMR, ^{13}C NMR, ^{1}H NMR, FT-IR and ESI-MS. Hence, POMs **10-12** were used as co-monomers along with methyl methacrylate (MMA) and ethylene glycol dimethacrylate (EDMA). The polymerization reactions were carried out with the help of porogenic solvents such as 1,4-butanediol and 2-propanol employing 1,1'-azobis(cyclohexanecarbonitrile) (ABCN) at 90°C as radical initiator (Scheme 4b). The resulting polymers were characterized in the solid state by means of FTIR, TGA, TEM, SEM, and EDX, with this latter evidencing a highly homogeneous distribution of the POM units within the polymer matrix. Interestingly, the presence of POM moieties inside cross-linked porous polymers favored high degrees of swelling and a gel-like behavior. The introduction of POM into processable polymer matrices is of interest for the development of heterogeneous catalyst systems to be employed in continuous processes based on fixed-bed reactors and membrane reactors. In this regard, polymers **PMMA-13-15** succeeded as catalysts for the activation of hydrogen peroxide for oxygen transfer, as demonstrated by the quantitative and selective oxidation of methyl *p*-tolyl sulfide, resulting **PMMA-14** the most promising. Next, this polymeric material has been further employed for two-step oxygen transfer to dibenzothiophene, a valuable protocol for fuel cleaning via oxidative desulfurization. The **PMMA-14**

removes sulfur-based compounds from n-octane in 90 min and reduces the sulfur content to about 10–8 ppm, confirming the promising potential of supported polyoxometalates in this field.

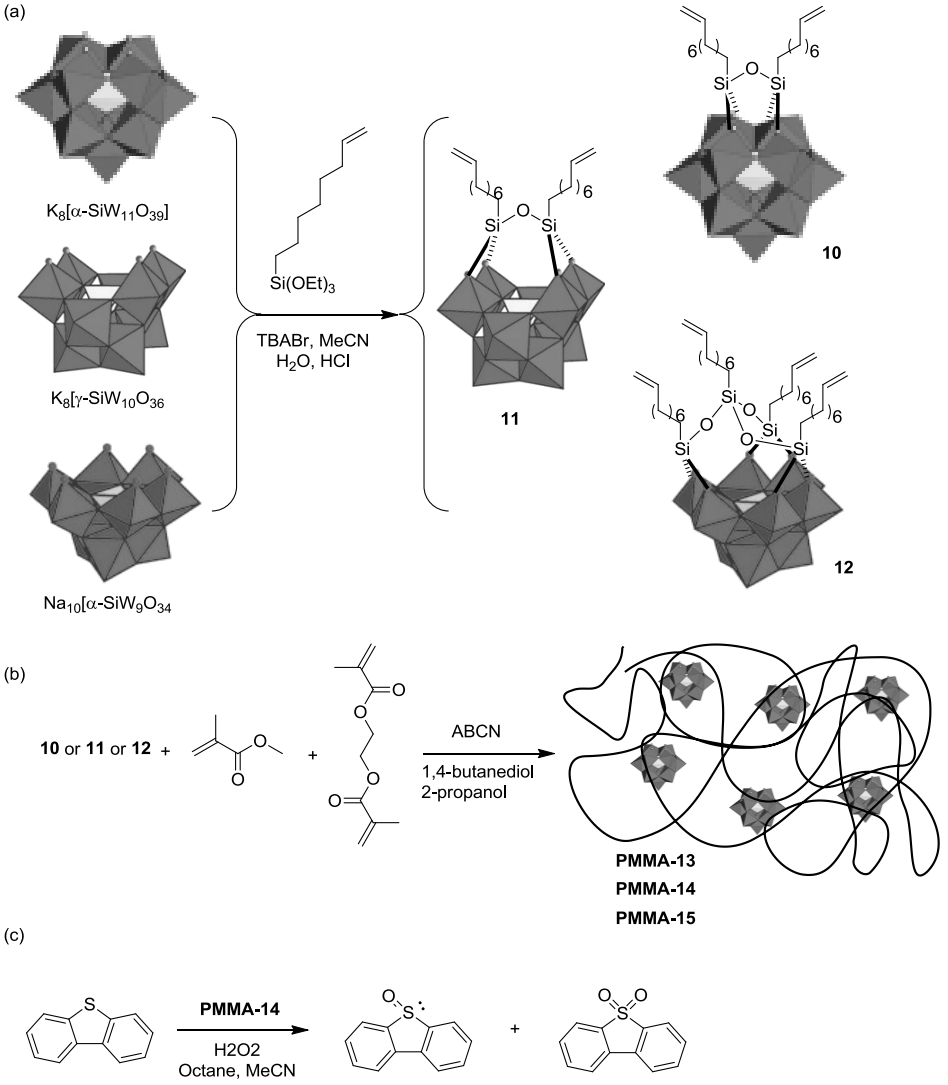

Scheme 4. Synthesis of (a) hybrid polyanions **10**-**12**, (b) the corresponding cross-linked PMMA polymers, and (c) two-steps oxidation of dibenzothiophene.

2.2 METAL-ORGANIC FRAMEWORKS

Metal-organic frameworks (MOF) are a recent class of porous polymeric material, constructed mainly by coordination bonds between metal ions and organic bridging ligands, and are at the interface between molecular coordination chemistry and materials science. A plethora of novel structures has been prepared which feature amongst the largest pores known for crystalline compounds. Such porous networks that contain empty space where guest molecules are occupied are of particular interest because they have great potentials to be applied in molecular adsorption and separation processes, ion exchange, catalysis, sensor technology, and opto-electronics.

An example of superb organic-inorganic crystal engineering control has been very recently reported in which a homogeneous series of oligophenylenes with two-to-seven, nine and eleven phenyl units (**16-24**, Fig. 5) have been employed as links for the systematic expansion of isoreticular metal-organic frameworks (IRMOFs).[5]

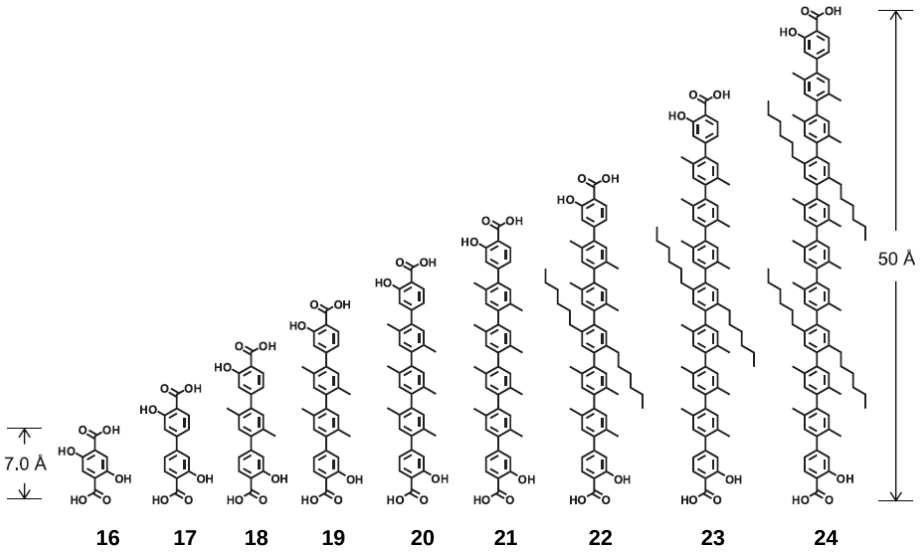

Fig. 5. Chemical structure of organic links **16-24** used in the synthesis of a series of nine IRMOFs

The synthesis of links **16-24** required a modular synthetic strategy and, especially for the longer molecules, reiterative Palladium-mediate catalyzed cross-coupling reactions which enabled the efficient preparation of the present series of organic links with lengths ranging from 7 (**16**) to 50Å (**24**) (Fig. 5). In such a way gram quantities of soluble organic links **17** to **24** were synthesized in 5 to 16 steps. Hence, the MOF were prepared by dissolving $Mg(NO_3)_2 \cdot 6H_2O$ [or $Zn(NO_3)_2 \cdot 4H_2O$] and the link in DMF and,

after leaving reacting for 12 hours in an isothermal over at 120°C without stirring, usually crystals in 60-95% of yield were collected.

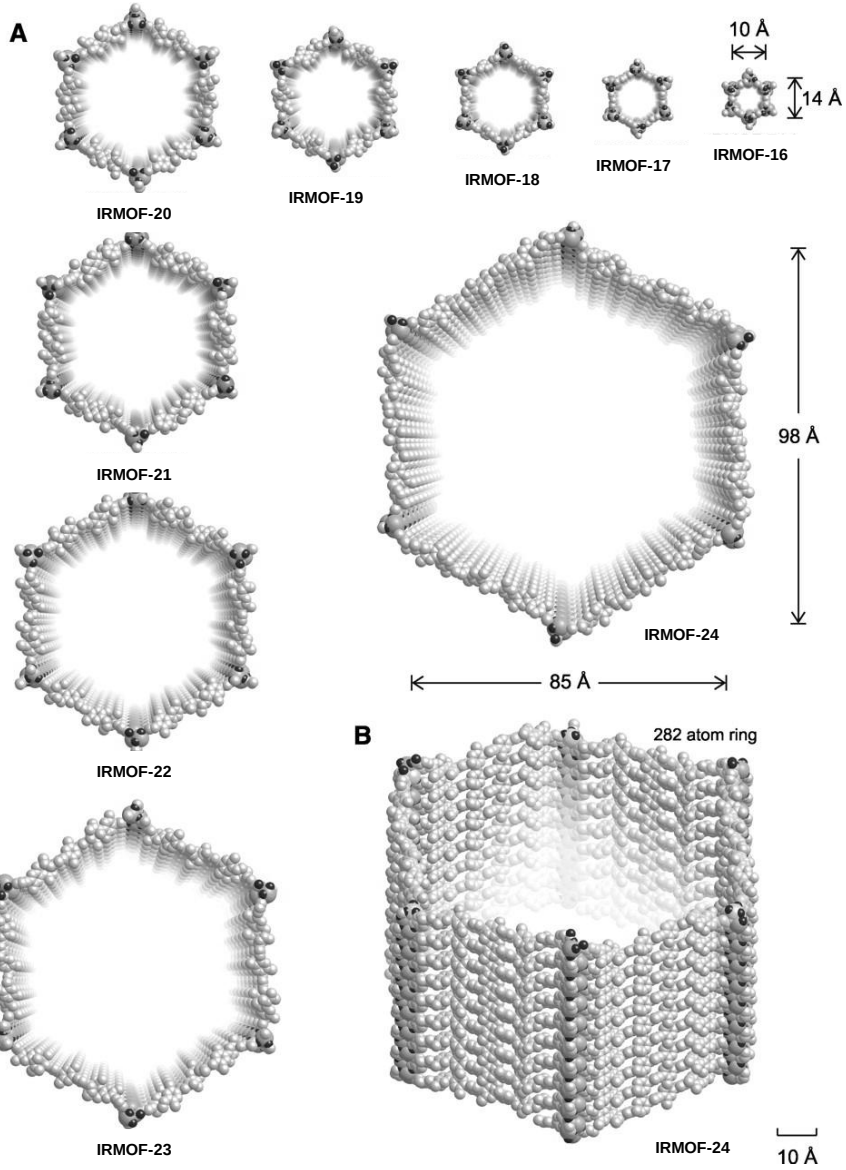

Fig. 6. Crystal structures of IRMOF series: (a) Perspective views of a one-dimensional channel shown for each member of IRMOF series. (b) Perspective side view of the hexagonal channel, showing the ring of 282 atoms that define the pore aperture of **IRMOF-24**. Reprinted with permission from ref. 5. © 2012 AAAS.

The so-obtained IRMOF series has been characterized by means of powder X-ray diffraction, solid-state ^{13}C MAS NMR, FT IR, EA, TGA, TEM and SEM. The pore aperture, defined as the length of the diagonal and the distance between the two opposite edges in the regular hexagonal cross section (Fig. 6a), for the IRMOF series ranges from 14 to 98Å, being this latter the largest ever reported. As expected, very high values for BET surface areas measurement has been determined (for **IRMOF-19** 2480 $m^2\ g^{-1}$). Once demonstrated their stability, porosity and extremely large-pore-aperture, IRMOF have been employed as new hosting superstructures for especial guests: hence **IRMOF-19** uptakes vitamin B12 from its solution, **IRMOF-20** hosts a 5 nm sized metal-organic polyhedral, **IRMOF-22** accommodates myoglobin and **IRMOF-24** is able to contain the green fluorescent protein (GFP), whose characteristic fluorescence remains unaltered after inclusion. In the next future these new materials could be applied as recyclable nanoreactors for biocatalysis.

But MOFs can be efficiently employed in heterogeneous catalysis. A nanotubular MOF was synthesized by linking up the bent organic ligand **25** and tetra-coordinated zinc cations under mild conditions.[6] Structural analysis revealed that **MOF-25** has a very large exterior wall diameter of 4.91 nm and an interior channel diameter of 3.32 nm (Fig. 7). Interlocking of the nanotubes gives rise to a 3D chiral framework containing 1D helical cylindered channels with diameter of 2.0 nm.

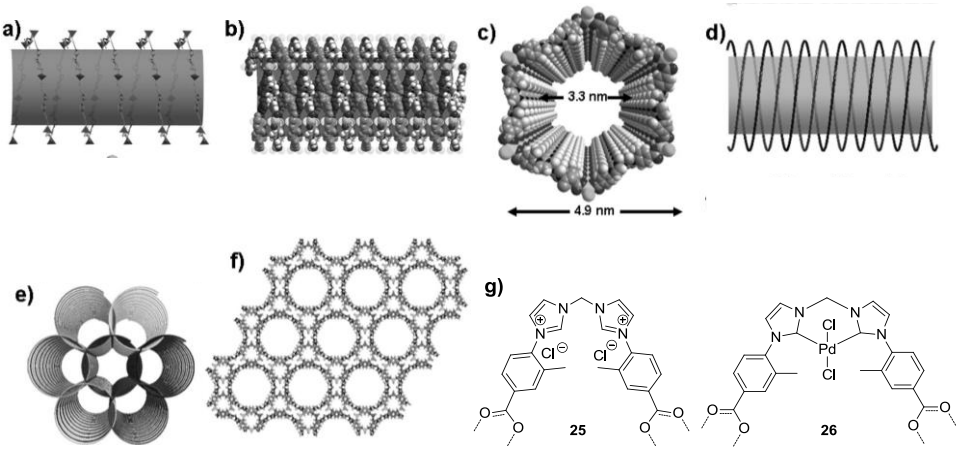

Fig. 7. (a) Side-view of the right-handed helical chain. (b) Space-filling representation of the nanotubular **MOF-25**. (c) Perspective view of the open-ended hollow nanotubular MOF. (d) Schematic representation of the double-helices. (e) Schematic representation of intertwined nanotubes. (f) Packing diagram of **MOF-25**, showing the 1D opening channels as viewed along the *c* axis. (g) Bent organic links **25** and NHC **26**. Reprinted with permission from ref. 6. © 2012 ACS.

Subsequently, **MOF-25** has been post-functionalized with $Pd(AcO)_2$ which led to the formation of the corresponding *N*-heterocyclic carbene form (**MOF-26**). The two parent MOFs were characterized by single X-ray diffraction analysis, PXRD, TGA and TEM. Moreover, XPS analysis on **MOF-26** showed that no Pd nanoparticles were formed during post-modification and all the palladium is in its oxidized form, whilst inductively coupled plasma mass spectrometry (ICP-MS) revealed a Pd content of 7.8%. The nanoporous nature of the MOF-NHC make it suitable for high performance catalysis. In this regard **MOF-26** did not disappointed, just 0.5 mol% (based on Pd) were sufficient to smoothly promote C-C bond forming both in Suzuki and Heck coupling reactions with quantitative yields (Scheme 5a-b).

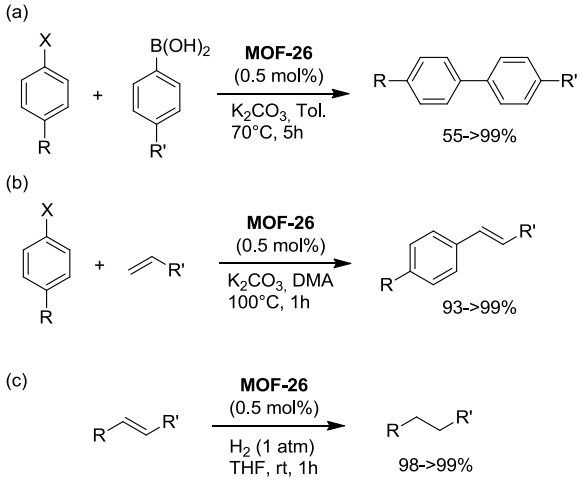

Scheme 5. Coupling and reduction reactions promoted by **MOF-26**.

In addition, **MOF-26** revealed to be an efficient and versatile catalyst also in reduction processes. Indeed complete hydrogenation of olefins has been carried out in just 1h with 0.5 mol% of catalyst, and the same amount it was able to completely reduce nitrobenzene into aniline. In addition all the processes were repeated recovering and recycling the catalyst for 6 consecutive cycles without losses in activity. Interestingly. The synergistic effect of combing the components into the MOF architecture was proven by the fact that the components alone never reached the levels of activity of the superstructure.

Post-synthetic modification of MOF has been also followed in order to prepare opposite enantiomorphs able to act as organocatalysts. Firstly, a metal-organic framework, **MOF-27**, endowed with triple bonds has been easily prepared (yield 65%) and subsequently subjected to Huysgen's click reaction (yield 80%) with *L*- or *D*-2-azidomethylpyrrolidine affording *L*- or *D*-**MOF-28** (Scheme 6).[7]

Crystal analysis of **MOF-27** displayed the positions of the clickable alkyne moieties are well exposed within the 1D channels. MOFs were characterized by means of PXRD, TGA elementary

analysis and NMR. In addition, circular dichroism spectra of *L*- or *D*-**MOF-28** showed, as expected, opposite Cotton effects for the enantiomers.

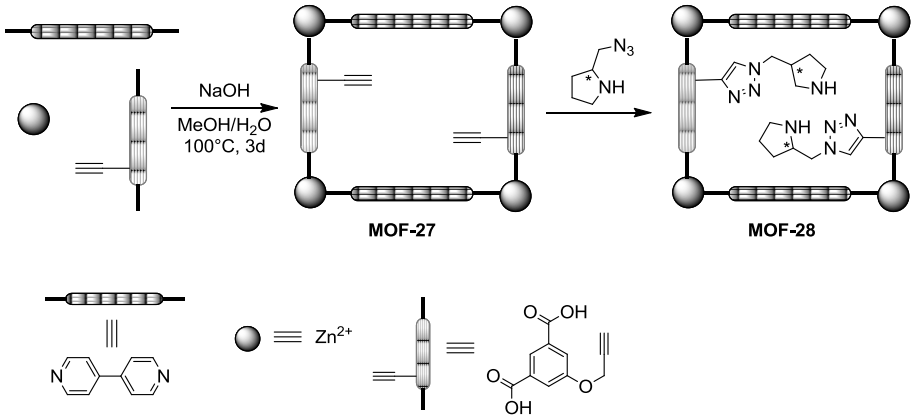

Scheme 6. Schematic drawing of alkyne modified **MOF-27** and **MOF-28** endowed with chiral (*L*- or *D*-2-triazolomethylpyrrolidine) after click reaction.

Next, *L*- or *D*-**MOF-28** have been employed as catalyst in asymmetric aldol reactions between aromatic aldehydes and cyclohexanone in MeOH/H_2O mixture (Scheme 7). Yields and enantioselectivity were from moderate to fair, and rather large reaction times were needed (7 days). What is interesting here is that once again a synergistic effect in the hybrid catalytic material can be noticed. Indeed, the components alone were not able to promote aldol reaction nor to reach the same selectivity (26% vs 70% ee). Catalysts were recovered and recycled three time with little loss in activity.

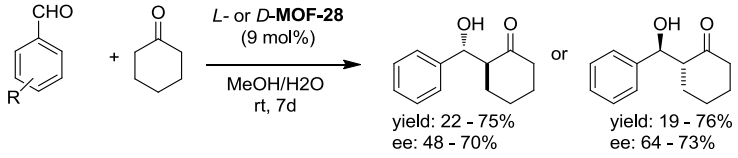

Scheme 7. Asymmetric aldol reaction catalyzed by *L*- or *D*-**MOF-28**.

More recently, two enantiomeric MOFs have been obtained when tris(4-(1-(2-pyridin-2-ylhydrazono)ethyl)-phenyl) amine **31** and $AgBF_4$ were reacted in methanol in the presence of 10 mol% of (+)-cinchonine or (-)-cinchonidine which acted as chiral template in the growth of homochiral crystals MOF (Scheme 8).[8] The crystallographic analysis of *P*- and *M*-**MOF-32** revealed that the two Shiff base ligands chelate the silver(I) atom in a distorted tetrahedral geometry with a dihedral angle between the bidentate chelating rings of 49.4° (Fig. 8). Moreover, the chirality of the material ligand proceeds also from the atropisomeric chirality of the thiphenylamine cores (torsion angle of about

74.5°). Solid state circular dichroism spectra of *P*- and *M*-**MOF-32** displayed opposite Cotton effects for the two enantiomeric materials.

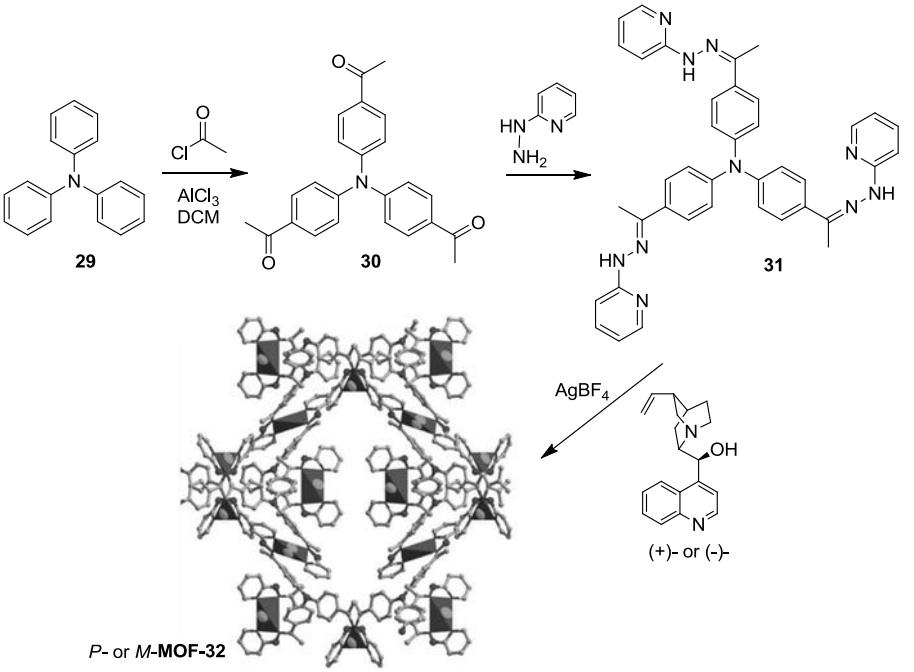

Scheme 8. Synthetic strategy for the synthesis of *P*- or *M*-**MOF-32**.

The catalytic activity of the chiral solid *P*-**MOF-32** was assessed by asymmetric 1,3-dipolar cycloaddition reactions involving methyl-2-(benzylideneamino)acetate and *N*-methylmaleimide (Fig. 8c). For three consecutive cycles, a catalyst loading of 3 mol% (9 mol% based on silver(I) ions) led to a yield of 90% with an enantioselectivity of 90% after 24 hours. The reaction gave almost exclusively the endo adduct in all cases. The high enantioselectivity may originate from the restricted movement of the substrates within the confined microporous systems. Under identical experimental conditions *M*-**MOF-32** showed similar catalytic activities (88% of yield) but gave products with opposite chirality (82% ee).

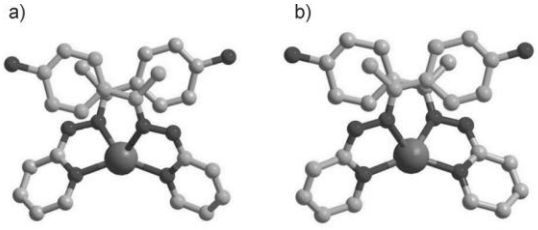

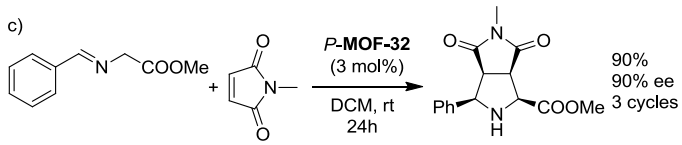

Fig. 8. Chiral configuration of the silver centers for a) *P*-**MOF-32**; b) *M*-**MOF-32**; c) asymmetric 1,3-dipolar cycloaddition of methyl-2(benzylidene amino)-acetate with *N*-methylmaleimide promoted by *P*-**MOF-32**.

2.3 AMORPHOUS AND MESOSTRUCTURED HYBRID SILICA

Amorphous and mesostructured silicas are well known materials that can be prepared and modified by means of sol-gel techniques. For most of these porous materials, modifications of the inorganic backbone are required to provide a certain specific surface chemistry or active sites on the inner pore surface. This makes the materials more viable for applications in catalysis, sensing or separation technologies, for example. In principle, the materials can be functionalized by simple inclusion of active species in the confined pore spaces, but in many cases covalent anchoring of functional moieties (mostly organic or organometallic) is required to avoid leaching.

The nature of hybrids obtained by sol-gel can be extremely diverse since the number of potential precursors is very high. One of the most significant characteristics of the sol-gel processes, that is of crucial importance from the point of view of enabling applications, is related to the easy processing of these materials, such as films, monoliths, fibers, or powders with particles of controlled size and shape which can in turn be applied in HPLC columns or in fixed beds for continuous flow processes.

Although modified silicas have been employed in a widespread of fields herein we will show selected examples in asymmetric catalysis. Generally speaking, covalent immobilization of a catalyst enables for its recover and recycle, whenever it is not degraded during the reaction, but also allows to explore new solvent profiles impossible to be explored under homogeneous conditions. However, heterogeneization should be carried out for those catalysts which display a wide range of application in several processes since the immobilization strategy involves several additional synthetic steps. In this regard, recently the versatile organocatalyst 5-(pyrrolidin-2-yl)tetrazole has been supported for first time.[9] Previously this costly and time consuming catalyst was not recovered after catalysis. The synthetic strategy starts with the quantitative conversion of (2*S*,4*R*)-*N*-Boc-4-O-allyl-hydroxyproline **33** to the corresponding amide **34** by in situ activation of the carboxylic acid (Scheme 9). Subsequent dehydration promoted by cyanuric chloride gave the corresponding nitrile **35** in high yield (82%), which in turn was transformed into the tetrazole **36** (85%) by cycloaddition with sodium azide. Then photoinduced thiol–ene coupling was chosen for the covalent linking of **36** to a modified-silica gel

endowed with mercaptopropyl groups (1.05 mmol/g) after sol-gel reaction with (3-mercaptopropyl)-trimethoxysilane in refluxing toluene. After immobilization, the Boc has been removed by acid treatment with TFA, affording the desired heterogeneous material **38** with a loading of 0.76 mmol/g of catalyst.

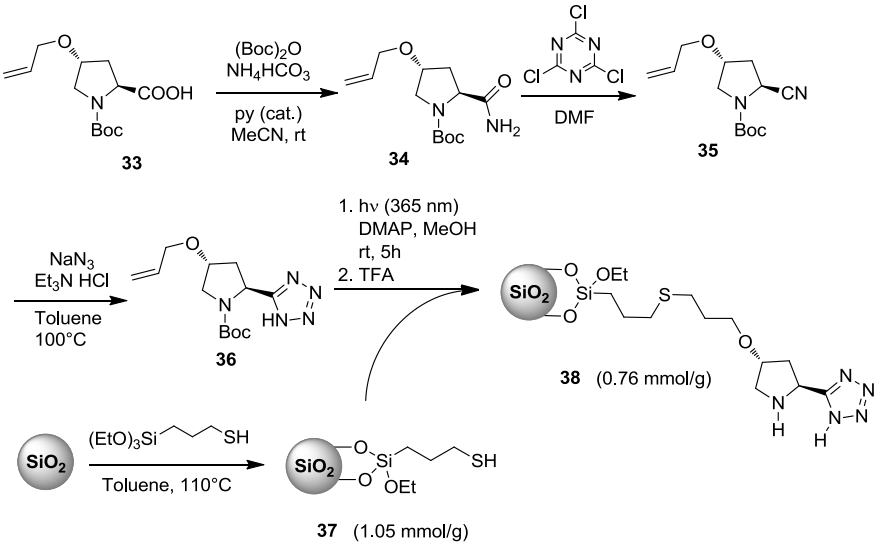

Scheme 9. Preparation of silica-immobilized 5-(pyrrolidin-2-yl)tetrazole **38**.

Next the hybrid silica has been employed as catalyst in asymmetric processes. Noteworthly, the hybrid material is able to reproduce the catalytic versatility of the parent unsupported version. In fact **38** successfully worked in four different asymmetric processes in which new C-C and C-N bonds were formed along with the creation of new stereocenters (Scheme 10). Hence, aldol, Michael, Mannich and α–amination reactions were performed employing 10 mol% of heterogeneous catalyst with high levels of conversion and selectivity. This success prompted to prepare a packed-bed microreactor by filling a stainless steel column with tetrazole-functionalized silica catalyst **38** which was in turn used in the continuous-flow aldol reaction of cyclohexanone with *p*-nitrobenzaldehyde. After optimization studies, the temperature of microreactor resulted to be a key factor for the efficiency of the flow process. Heating the microreactor at 50°C resulted in complete conversion of the aldehyde and the stereoselectivity was not compromised. Moreover, no formation of dehydration by-product allowed the isolation of the aldol product by simple evaporation of the solvent and excess cyclohexanone. Then a series of aromatic aldehydes has been investigated and the microreactor showed some deactivation only after 120 h of work.

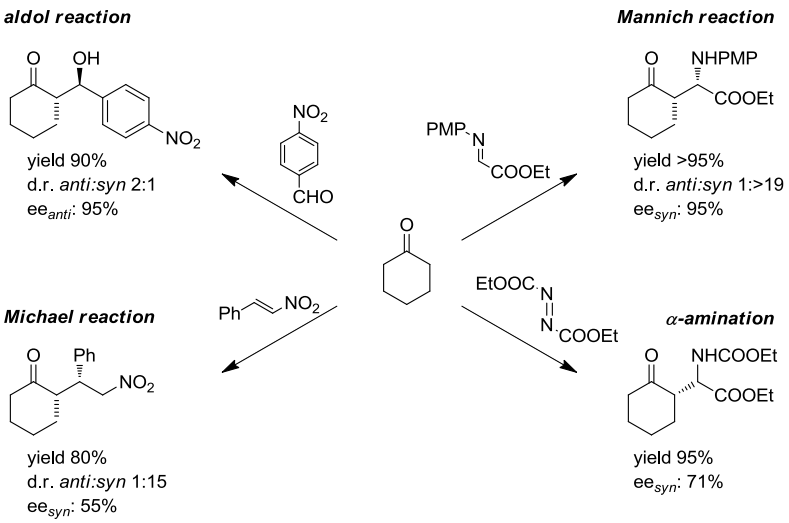

Scheme 10. Asymmetric reactions organocatalyzed by 10 mol% of **38**.

Beside silica post modification, other different convenient methods for the preparation of organosilica materials with targeted properties are the sol–gel hydrolytic condensation of organo-alkoxysilanes and the surfactant-assisted sol–gel synthesis of a mesostructured silica. These are commonly employed routes for the synthesis of mesostructured porous organosilicas with a controlled loading of the functionalizing fragment on the support. These materials usually show high surface areas and large pore sizes that can favor both accessibility to the organic functions and diffusion of the solvent–soluble reactants within the solid, basic for efficient liquid–solid phase catalytic reactions. These approaches have been followed for the immobilization of a prolinamide in order to discern the effect of amorphous of mesostructured supports on the catalysis. The synthesis has been accomplished according to Scheme 11: aminoindane-derived prolinamide **40** was obtained by condensing *N*-benzyloxycarbonyl-4-*trans*-hydroxy-L-proline **39** and (*R*)-2,3-dihydro-1*H*-inden-1-amine. Then, reaction with (3-isocyanatopropyl)triethoxysilane provided the silylated Cbz- prolinamide followed by the removal of the protecting group afforded **41** with good overall yield. Hybrid silica materials were then prepared following three different routes for the immobilization of prolinamide derivative **41**: (i) common nucleophilic-catalyzed sol–gel hydrolysis-condensation with two different molar ratios of TEOS:3 (5 and 19) yielding a non-porous (**42**) and a mesoporous (**43**) hybrid materials respectively; (ii) with a neutral surfactant as structure-directing agent affording the worm-like mesoporous material **44** and (iii) grafting of **41** on a SBA-15 silica, yielding preserved mesostructured **45**.

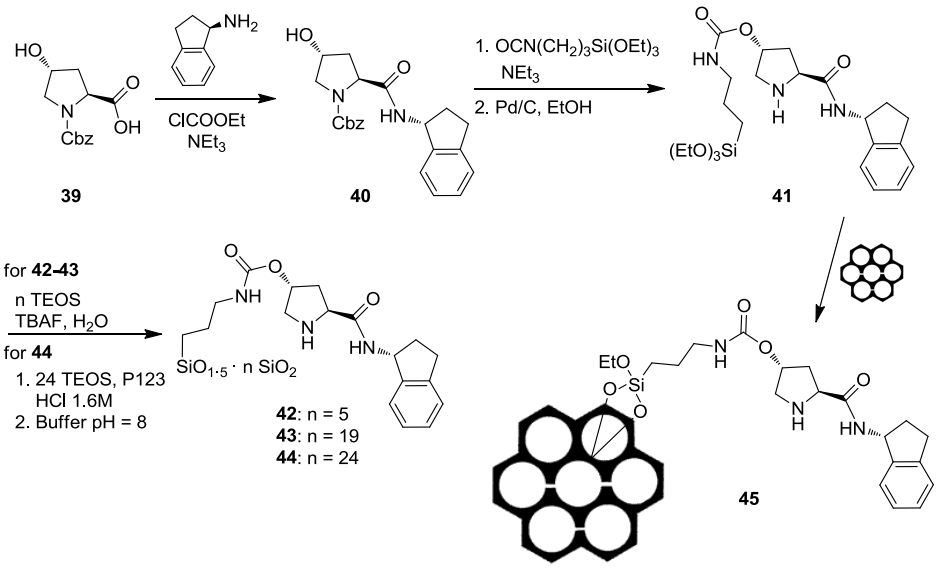

Scheme 11. Synthesis of prolinamide **41** and the different routes for its immobilization

The prepared materials were characterized by elemental analysis, ^{29}Si CP MAS solid state NMR, IR, TGA, TEM, SEM, PWRD and nitrogen-sorption measurements. Due to the low amount of TEOS used in the synthesis, N_2-sorption experiment showed the non-porous nature of **42**, whereas high surface areas presented **43-45** (450, 300 and 360 m^2 g^{-1}, respectively). The catalytic activity of the new hybrid materials was evaluated in the direct asymmetric aldol reaction between *p*-nitrobenzaldehyde and cyclohexanone in water. All the materials presented quite good activity and, surprisingly, some improved enantioselectivity compared to the homogeneous prolinamide. Although some of them, **42** and **45**, were recycled up to five times with low variations in yields and stereoselectivity, increasing of the porosity does not affected neither the yield nor the selectivity.

On the other hand, hydrolysis-condensation of 1,3-bis(3-(triethoxysilyl)-propyl)-1*H*-imidazol-3-ium iodide **46** alone led to the creation of an imidazolium based organic–inorganic hybrid silica network with marked phase-transfer properties. To this material a (*S*,*S*)-TsDPEN-derived silane has been grafted and catalyst **47** was then obtained by complexation with $(Cp^*IrCl_2)_2$ (Scheme 12).[10] The successful incorporation of Iridium catalyst has been confirmed by TGA and inductively coupled plasma (ICP) analyses (29 mg Ir per gram of material) as well as by solid-state ^{13}C CP MAS NMR. In addition, the ^{29}Si CP MAS NMR revealed the presence of a uniform organosilicate framework with $RSi(OSi)_3$ (R = chiral Cp*IrTsDPEN functionality) as the main part of the silica hybrid material. Finally, TEM image

with chemical mapping indicated that catalyst **47** was composed of micrometer-sized particles with uniformly distributed iridium centers within the nanostructures.

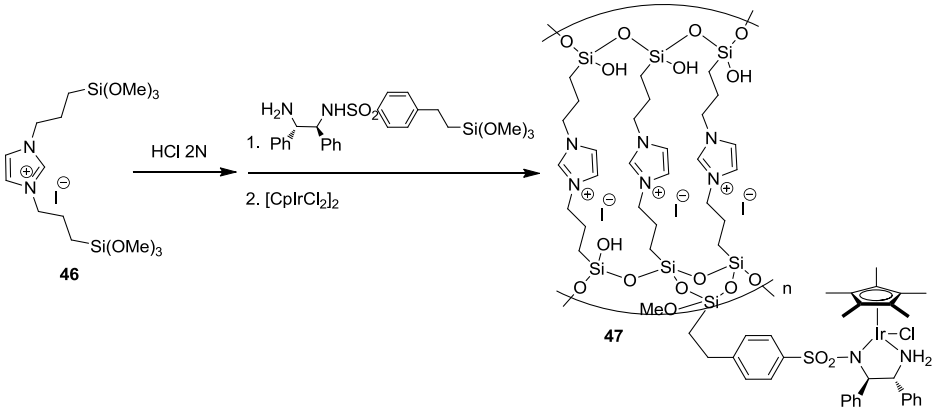

Scheme 12. Preparation of hybrid catalityc silica **47**.

Then, the catalytic performances of hybrid silica **47** have been tested in the asymmetric transfer hydrogenation of a series of ketones with sodium formate without addition of Bu_4NBr as a phase-transfer catalyst in aqueous medium (Scheme 13). In general, just 0.1 mol% of catalyst (based on Ir content) gave rise to quantitative conversions and high enantioselectivities for all tested ketones. It is interesting to note that the ester moiety can be tolerated in a ketoester but, most importantly such catalyst performed better and faster than the homogeneous counterpart demonstrating that the imidazolium functionality have a synergistic effect with the organometallic part enhancing its catalytic activity. Hybrid **47** could be recycled for 10 consecutive cycles without losses in activity and selectivity with only a minor leaching of 0.6% of Ir per cycle.

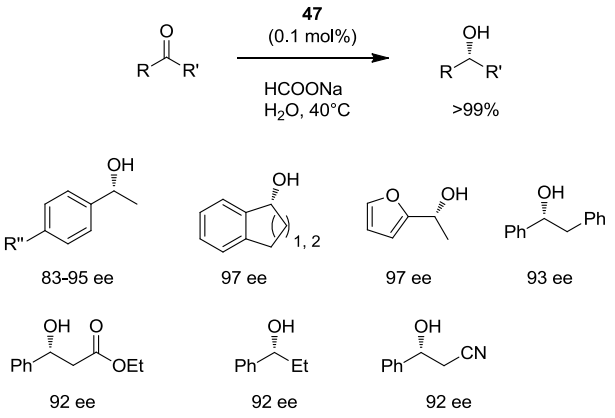

Scheme 13. Asymmetric transfer hydrogenation of ketones mediated by catalyst **47**.

Analogously to catalyst **47**, similar Rhodium complexes have been immobilized onto mesostructured silicas by post-grafting or by surface-bound triflate encapsulation (Scheme 14).[11] In this latter case ion-pairing has been the strategy of choice for the immobilization of catalyst **48** onto the channels of methylated SBA-15 and SBA-16 structured silicas. Methylation has been carried out during the synthesis of such supporting materials by means of hexamethyldisilazane in order to cap silanol groups present in the outer part of the channels while these latter were occupied by the templating polymer. Permethylation was necessary to avoid that the triflate group of **48** would interact with the external sylanol group instead of coordinating the inner OH groups. The encapsulation take place by leaving **48** to diffuse within the pores of Me-SBA-16 and Me-SBA-16, then the leaching is avoided by tailoring pore entrance with diphenylsilyldichloride. Grafting of silylated-precursor **51** led to the covalently immobilized catalyst **52**.

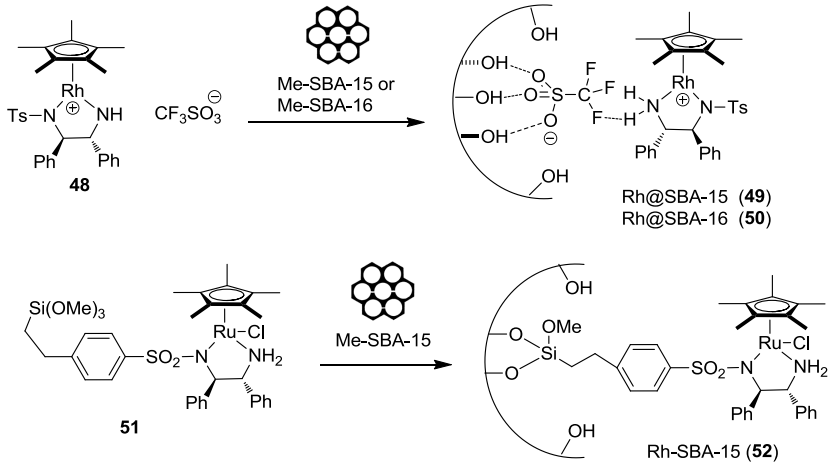

Scheme 14. Ion-pair encapsulated and grafted Rhodium catalysts **49**-**50** and **52**.

For hybrids **49** and **50** ICP and elemental analyses were in complete agreement indicating a loading of 0.110 and 0.067 mmol/g. The successful incorporation of cationic **48** within Me-SBA-15 and Me-SBA-16 channels has been confirmed by solid-state ^{13}C CP MAS NMR spectra (Fig. 9). Heterogeneous catalysts **49**-**50** exhibit the typical peaks of TsDPEN moiety [21 ppm for Ar-CH_2, 69-72 ppm for N-CH-Ph and 126-136 ppm for C_6H_5] and the typical peaks of $CpMe_5$ moiety (96 ppm for C5 and 8-10 ppm $CpCH_3$). The same occurred for **52**. The ^{29}Si CP MAS NMR spectra indicated the presence of strong Q3-Q4 peaks in materials **49**-**50** stemming from the inorganosilicate frameworks with $(HO)Si(OSi)_3$ and $Si(OSi)_4$ as the main networks. The relatively weak D signal corresponding to -$SiCPh_2$ groups and the relatively weak T signals derived from -$SiCMe_3$ groups suggested that these groups were bonded onto the external walls of the inorganosilicate frameworks. TEM and XRD

confirmed the ordered two-dimensional hexagonal (SBA-15) and cubic (SBA-16) distribution of the porous channels. Surface areas were in the 300-410 m^2/g range and maintained quite high values even after functionalization and partial capping.

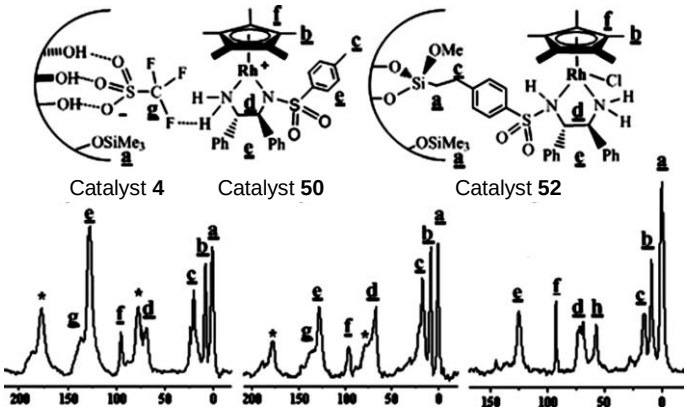

Fig. 9. ^{13}C CP MAS NMR spectra of **49**-**50** and **52**. Reprinted with permission from ref. 11.
© 2012 John Wiley & Sons.

Then the hybrid materials were applied as asymmetric catalysts in the ultrasound promoted asymmetric transfer hydrogenation of aromatic ketones (Scheme 15). The use of ultrasounds resulted a highly convenient method in enhance greatly catalytic activity probably due to a cavitation effect and shock wave. The cavity collapse derived from the cavitation effect was beneficial to expose fresh, highly active surfaces while the associated shock waves improved significantly the mass transfer. The main effect was the reduction of reaction time to 20-30 minutes for the quantitative conversion of ketones to the corresponding alcohols still maintaining the high levels of enantioselectivity of Rh-catalysts. Moreover, in recycling studies **50** nicely worked for up to ten cycles.

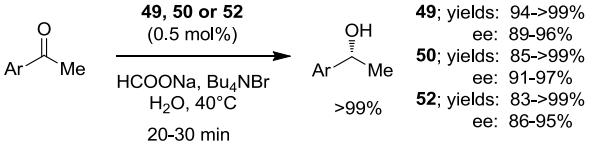

Scheme 15. Asymmetric transfer hydrogenation of ketones catalyzed by **49**-**50** and **52**.

2.4 MAGNETIC NANOPARTICLES

Magnetic nanoparticles, MNP, are of great interest in a wide range of disciplines, including magnetic fluids, catalysis, biotechnology/biomedicine, magnetic resonance imaging, data storage and

environmental remediation. Hence, functionalized nanoparticles are very promising for applications in catalysis, biolabeling, and bioseparation. Especially in liquid-phase catalytic reactions, such small and magnetically separable particles may be useful as quasi homogeneous systems that combine the advantages of high dispersion, high reactivity, and easy separation. Various chemical methods can be used to synthesize MNP such as microemulsions, co-precipitation, sol-gel syntheses, sonochemical reactions, hydrothermal reactions, hydrolysis and thermolysis of precursors. But for real applications of MNP it is often necessary to coat with stabilizers or to functionalize them with functional groups like carboxylates, phosphates, and sulfates, all of them able to bind to the surface of magnetites.

One of the easiest way to achieve hybrid magnetic materials is to entrap MNP in a polymeric network. In this regard a series of iron oxide and silica-coated iron oxide nanoparticles have been entrapped into a highly cross-linked poly-ionic liquid network (Scheme 16).[12] The former were prepared by flame spray pyrolysis (FSP) of iron(III) acetylacetonate, whilst MNP-SiO_2 (23 wt% SiO_2-coated Fe_2O_3) were prepared by FSP of iron(III) acetylacetonate in xylene–acetonitrile solutions and the resulting aerosol was in situ coated with silicon dioxide by oxidation of swirling hexamethyldisiloxane vapour. The hybrid materials were then obtained by cross-polymerizing bis-vinylimidazolium salts **53-55** with AIBN in the presence of the MNP.

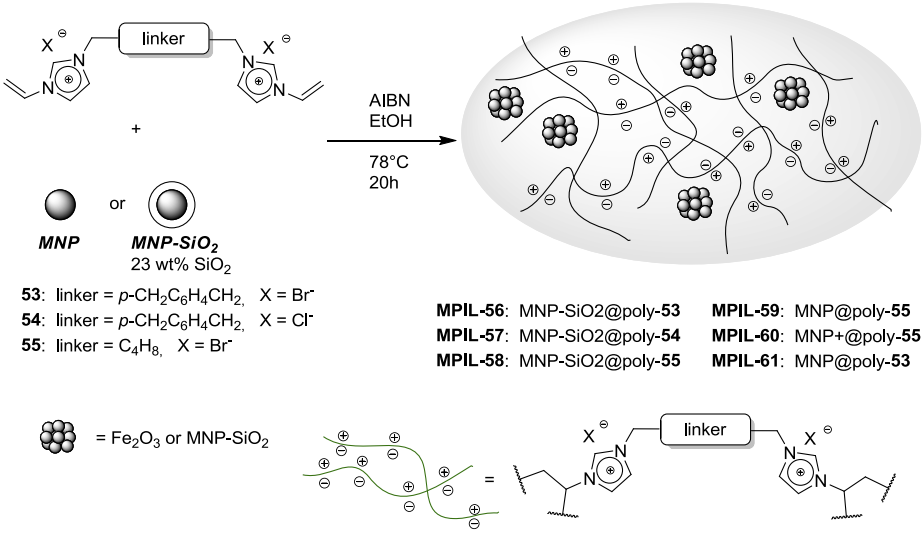

Scheme 16. Synthesis of magnetic nanoparticles encapsulated in highly cross-linked imidazolium networks.

The so-obtained magnetic-poly ionic liquids (MPIL) where thoroughly characterized by elemental analysis, TGA, FTIR, SEM, TEM. This latter clearly showed that several MNP (10-50 nm) are

embedded into micrometric polymer-particles. The room temperature magnetization of the materials was measured by an alternating gradient-field magnetometer (AGM) and clearly indicated that all the prepared hybrids maintain superparamagnetic properties. The catalytic activity of MPIL was then tested both as intrinsic catalysts as well as suitable support for metallic species and organocatalysts. Firstly, MPIL-**56-61** were employed as heterogeneous catalysts in the formation of cyclic propylene carbonate from the addition of carbon dioxide to propylene oxide (Scheme 17a). As expected on the basis of the accepted reaction mechanism, supported imidazolium salts in which the counter ion is represented by bromide provide a higher epoxide conversion than those containing chloride. These differences reflected the nucleophilicity order of the anions. Although low to moderate yields were achieved, MPIL-**58** was recovered and recycled 4 times with unchanged results. Next, the ability of MPIL-**56** as magnetically recoverable scavenger was tested in the removal of palladium from an aqueous solution of Pd(II) compounds such as $Pd(OAc)_2$ and as anionic species ($PdCl_4^{2-}$), and a Pd(0) compound such as $Pd(PPh_3)_4$. No palladium was found in the remaining aqueous solution (ICP-OES). The high scavenger property of such materials is demonstrated by the fact that the final materials contained 10 wt% of Pd reducing the residual palladium level from 2000 ppm to <1 ppm, resulting superior to thiol- or amine-modified magnetic particles-based scavengers. Finally, MPIL-**56** was also employed as organocatalyst magnetically recoverable reservoir by adsorbing L-Proline on its surface so afford Pro@MPIL-**56**. This latter nicely worked as heterogeneous organocatalyst in the asymmetric aldol reaction between acetone and *p*-nitrobenzaldehyde (Scheme 17b). The separation of catalyst from the reaction mixture is easily accomplished by exposure to an external magnet. After 4 cycles the activity diminished from 90 to 70% of yield bat it can be easily restored by regenerating the catalyst content.

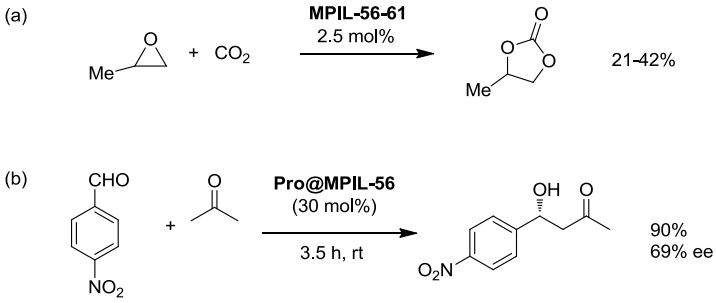

Scheme 17. a) addition of CO_2 to propylene promoted by MPIL; b) aldol reaction catalyzed by Pro@MPIL-**56**.

One of the most versatile and efficient organocatalysts is the MacMillan imidazolidinone. Recently this catalyst has been covalently immobilized onto MNP (Scheme 18).[13] MNP used as support were prepared by thermal decomposition of Iron(III) acetylacetonate in the presence of oleic acid,

oleylamine, and 1,2-dodecanediol as surfactants and showed a narrow size distribution (5.3 ± 1.4 nm). Hence, the grafting of 3-(azidopropyltrimethoxy)silane afforded the azide functionalized MNPs **62** which in turn reacted with the propargyloxy-substituted imidazolidinone **63** through copper-catalyzed alkyne azide cycloaddition affording the hybrid material **64** with a loading of 0.34 mmol/g.

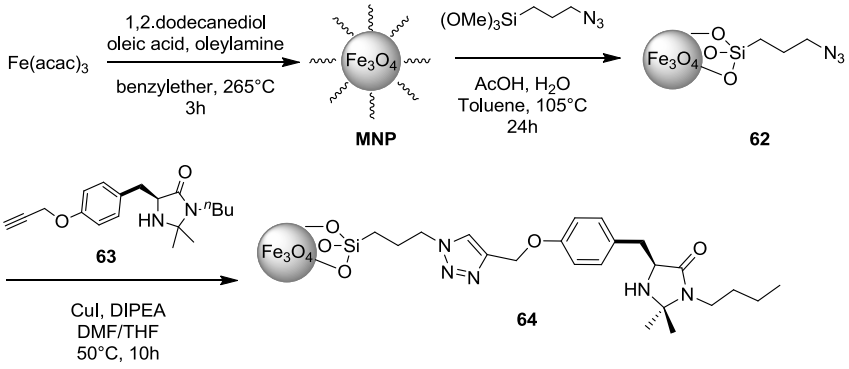

Scheme 18. Immobilization of the MacMillan catalyst onto MNP.

Then the modified magnetic nanoparticles were applied as catalyst in the asymmetric Friedel-Crafts alkylation of *N*-substituted pyrroles with α,β-unsaturated aldehydes at rt (Scheme 19). Although the catalytic activity was moderate to good, giving rise to yields in the 31-98%, good enantioselectivities were achieved and, most important, the easy magnetic recovery of the catalytic nanoparticles allowed a good recycle for 5 cycles.

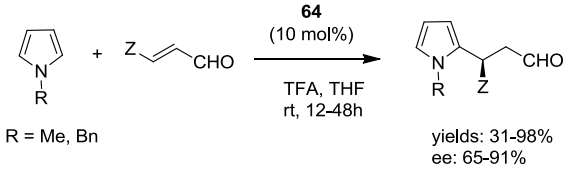

Scheme 19. Friedel_Crafts alkylation of *N*-Substituted pyrroles with α,β-unsaturated aldehydes promoted by 10 mol% of **64**.

Two novel Ruthenium-based organometallic catalysts have been prepared by employing different anchoring strategies to magnetic nanoparticles (Scheme 20).[14] Catalyst **67** has been synthesized by direct immobilization of a 4,4'-bisphosphonic acid-substituted BINAP-Ru-DPEN complex onto MNPs (loading 33 μmol/g). On the other hand, catalyst **69** has been prepared by following a stepwise strategy involving first the immobilization of 10-bromodecylphosphonic acid was onto MNPs, followed by

reaction with DPEN in anhydrous ethanol and then the coupling with freshly prepared [Ru(4,4'-$(TMS)_2$-BINAP)$(DMF)_2Cl_2$] to give the final superparamagnetic nanocatalyst (loading 5 μmol/g).

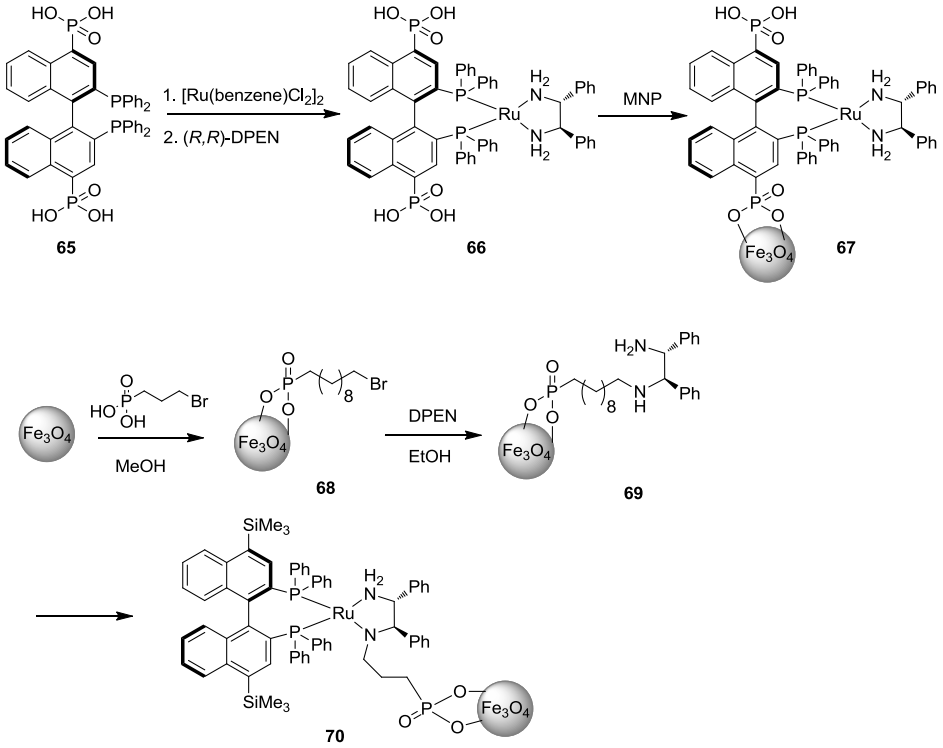

Scheme 20. Synthesis of Ru-based magnetic catalysts **67** and **70**.

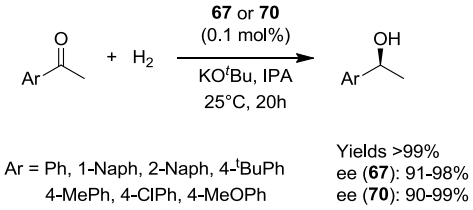

Scheme 21. Heterogeneous hydrogenation of aromatic ketones.

Both catalysts were employed in the heterogeneous hydrogenation of aromatic ketones with excellent results in terms of conversion and enantioselectivity (Scheme 21). Recycling studies on catalyst **67** displayed high reusability of such material for up to 10 cycles reaching the remarkable value of TON of 10,000. However, such hybrid cannot be vacuum dried nor left in a solvent for weeks since,

as showed by TEM, it strongly aggregates. This is very likely due to the presence of the second phosphonic acid moiety which favors the aggregation. On the other hand, **70** after the first cycle quickly deactivated, probably due to a redox side-reaction with the magnetite.

2.5 CARBON-BASED NANOFORMS

Carbon is a versatile and fascinating material that can be used in a number of technological processes, including high-tech processes. This is due largely to the ability of carbon atoms to bond with each other in various ways to form linear, planar, and tetrahedral bonding arrangements, thus producing materials with a large range of properties. Physicochemical characteristics such as electrical conductivity, surface area and porosity, and surface chemistry may be tuned for specific applications. In such a way the different nanoforms of carbon such as fullerenes, nanotubes, nanohorns, graphene and nanodiamonds, among others, are attracting a huge interest in the scientific community.

Single-walled carbon nanotubes (SWNTs) are molecular wires that exhibit interesting structural, mechanical, electrical, and electromechanical properties. A SWNT is unique among solid state materials in that every atom is on the surface. Surface chemistry could therefore be critical to the physical properties of SWNTs and their applications. The easiest way to exploit SWNTs' properties is to use it pristine but wrapped by proper polymeric chains. In this regard, recently SWNT have been wrapped by poly-ionic liquid chains of poly[1-(4-vinylbenzyl)-3-methylimidazolium tetrafluoroborate (PIL), forming a very stable homogeneous suspension.[15] The FTIR spectrum of the PIL-wrapped SWNTs confirmed the presence of the features of PIL and SWNTs. Then, the PIL/SWNTs suspension was drop deposited onto prefabricated interdigitated electrode patterns on a Si/SiO_2 substrate to prepare chemiresistive sensor devices (Fig. 10a). Hence, sensors were tested for gas detection displaying a remarkable dynamic response when exposed to different concentrations (500 ppt–50 ppm) of CO_2 (Fig. 10b). The sensitivity of the PIL/SWNTs sensor increases with respect to CO_2 concentrations ranging from 500 ppt to 50 ppm and a saturated tendency is observed at the concentration above 10 ppm (Fig. 10c). Importantly, by means of UV illumination, the sensor recovers to the baseline within 1 min. In addition, no significant change in the response sensitivity was observed when the device was exposed to 1 ppm CO_2 repeatedly, clearly indicating that the PIL/SWNTs networks-based sensors has good reproducibility and stability (Fig. 10d). Finally, the sensor proved to be also selective toward CO_2 detection when compared to other vapors such as CO, H_2, CH_4, ethanol vapor and water. The PIL/SWNTs sensor was not affected by the presence of water since a mixture CO_2 with 42% of relative humidity (RH) gives the same selectivity observed with dry CO_2 indicating that the sensor is highly resistant to moisture interference.

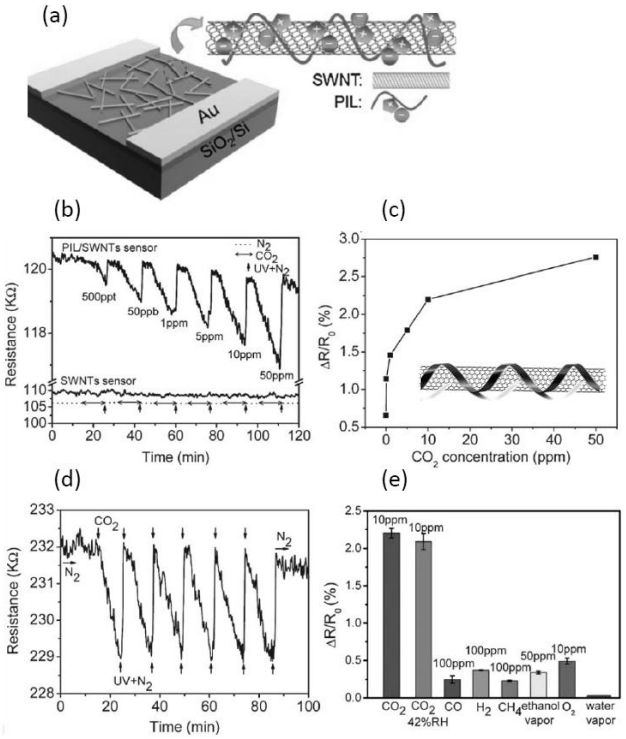

Fig. 10. a) Schematic illustration of the PIL/SWNTs-based sensor; b) dynamic response to different concentrations of CO_2 compared to that of a pristine SWNTs sensor; c) resistance change ($\Delta R/R_0$) with respect to different CO_2 concentrations; d) reproducibility in response to repeated exposure to 1 ppm CO_2; e) sensitivity toward CO_2, CO_2 + RH (42%), CO, H_2, CH_4, ethanol vapor, O_2 and water vapor (42% RH).

A different approach for the preparation of PIL-NT hybrids consist in the covalent linking and growth of the polymeric chains to the functionalized surface of the nanotube. This strategy has been recently reported and begins with oxidation of multi-walled carbon nanotubes (MWNTs) in order to produce nanotubes with several carboxyl groups (Scheme 22). The subsequent esterification with MeOH (sulfuric acid as catalyst) followed by aminolysis with 1-(3-aminopropyl)imidazole led to the imidazole-functionalized MWNTs **71** with a 0.4 mmol/g of loading.[16] The quaternization of imidazole moieties with allyl chloride afforded the material **72** which was used in two radical polymerization reactions promoted by AIBN: with 1-butyl-3-vinylimidazolium chloride **73** to give hybrid nanotubes **74** and with 3-(3-vinylimidazolium-1-yl)propane-1-sulfonate **75** to produce zwitterionic MWNT **76**.

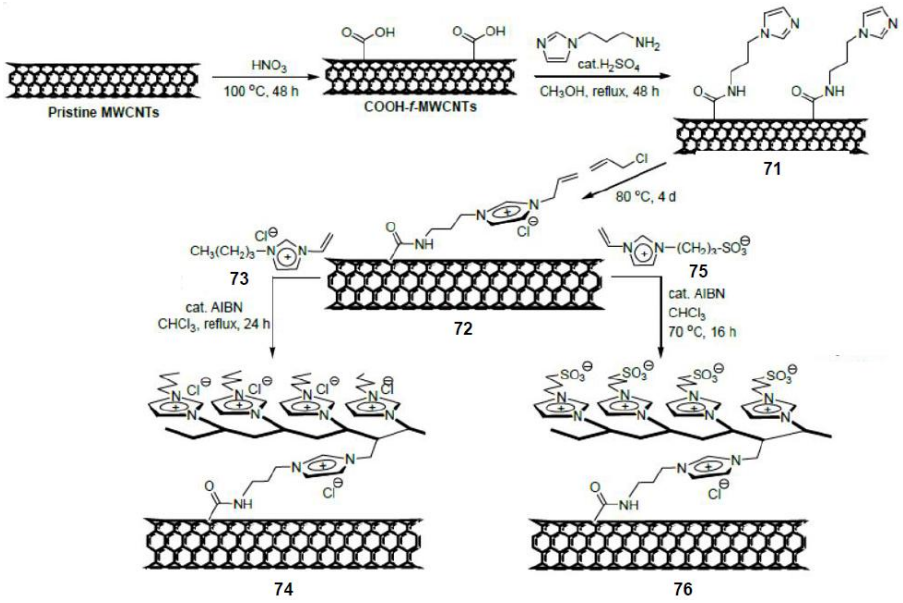

Scheme 22. Preparation of PIL-MWNT hybrids **74** and **76**.

Then, pre-synthesized sodium citrate-coated gold nanoparticles (AuNPs) were assembled onto poly(vinylbutylimidazolium chloride)-MWNTs **74** and zwitterionic poly(vinyl imidazoliumpropylsulfonate)-functionalized MWNTs **76**. In these latters, the imidazolium cation and the sulfonate anion are covalently bond in a molecule, which prevents intermolecular anion exchange allowing the charged AuNPs to assemble onto the NT surfaces through electrostatic interactions between zwitterionic imidazolium sulfonate and citrate ions. Conversely, in **74** the interionic reactions between imidazolium chloride and the sodium citrates give NaCl and imidazolium citrate salt, which produce naked AuNPs able to easy aggregate. Such behavior has been confirmed by TEM analysis where can be noticed that the AuNPs were not deposited onto the CNT surfaces, but were aggregated in the proximity of the NTs. Coversely, in the case of the zwitterionic **76** the AuNPs were densely decorated onto the NT surface without significant alteration of particle size to form supported AuNP@PIL-MWCNTs. The X-ray diffraction (XRD) patterns of these AuNPs showed typical face-centered cubic (fcc) Au diffraction patterns and the XPS confirmed the Au^0 oxidation state of the AuNPs. Finally, the electrocatalytic activity of the AuNP@PIL-MWCNTs assemblies for oxygen reduction has been successfully assessed.

Although the external functionalization of MWNTs allow for their modification, very often the loading obtained are quite low. A way to overcome to such drawback rely in the chemical

functionalization with dendrimers which exert a kind of amplification effect. Depending on the generation of dendrimer one can add 2, 4, 8 or even more peripheral groups per single MWNT-functionalization at once. In this light recently, polyamidoamine (PAMAM) dendrimers have been grown from the surface of MWNTs (Scheme 23).[17]

Pristine MWCNTs were firstly derivatized through a diazotization reaction, also called Tour reaction, using 4-[(N-Boc)aminomethyl]aniline and isopentylnitrate to form in situ an aryl-diazonium salt able to covalently undergo addition reaction to the NT sidewalls. Thus, acidic treatment (HCl/dioxane) allows the cleavage of the *tert*-butoxycarbonyl (Boc) protecting group leading to the amino functionalities (**77**) that could be further modified by polyamidoamine (PAMAM) dendron divergent growth. The PAMAM growth is an iterative two-step reaction that can give rise to a novel dendron generation each time the two-step functionalization cycle is iterated. This sequence consists first of a Michael addition between a methyl acrylate and free amino groups, followed by amidation of the peripheral ester units by ethylendiamine. In such a way MWNTs endowed with first generation (**78**) and second generation PAMAM dendrons (**79**) have been prepared. The four amino-groups per functionality in **78** were then alkylated by addition of glycidyl trimethylammonium chloride to achieve the desired positively charged d-MWCNTs·Cl **80**. These highly charged nanotubes can now accommodate negatively charged species through ion-pairing interactions and, in this case, the anion exchange reaction has been carried out with a negatively charged and highly luminescent Eu^{III} complex $[EuL_4]\cdot NEt_4$ **81**, in which L=(2-naphtoyltrifluoroacetonate). Characterization of **77-79** has been accomplished by TGA and TEM, whilst **80** and **82** were further analyzed by means of XPS, Raman, DOSY-NMR and photoluminescence (PL) studies. TGA of luminescent MWNT **82** revealed a loading of 0.08 mmol/g of Eu complex, in good agreement with the estimated dendron loading of 0.07 mmol/g of **80**. XPS analysis of d-MWCNTs·Cl showed the presence of Cl(2p) and N(1s) signals along with those of C and O, whereas in the MWCNTs·$[EuL_4]$ spectra Eu(3 d) (at 1135 eV) and F(1 s) (at 686 eV) resonances appeared along with the complete absence of Cl-centered resonances in the final hybrid material corroborating the effectiveness of the ion exchange reaction.

The emission profile of d-MWCNTs·$[EuL_4]$ **82** in KBr is identical to that of $[EuL4]^-$ **81** alone with an intense and characteristic peak at 615 nm. The excited-state lifetime in KBr is 0.29 ms for both d-MWCNTs·$[EuL_4]$ and $[EuL_4]\cdot NEt_4$. This indicates that neither quenching of the Eu^{III} complex by the MWCNTs framework through energy transfer, nor self-quenching between the lanthanide complexes themselves is occurring. Then, 0.005 w/w% dispersions of **82** in a commercial matrix of polymer (ESCORENE) in toluene were prepared and finally poured into shaped stamps The polymeric composite resulted very luminescent and shape-persistent, even under mechanical stress, and the luminescence resulted homogeneous despite the low loading of the emissive material in the composite.

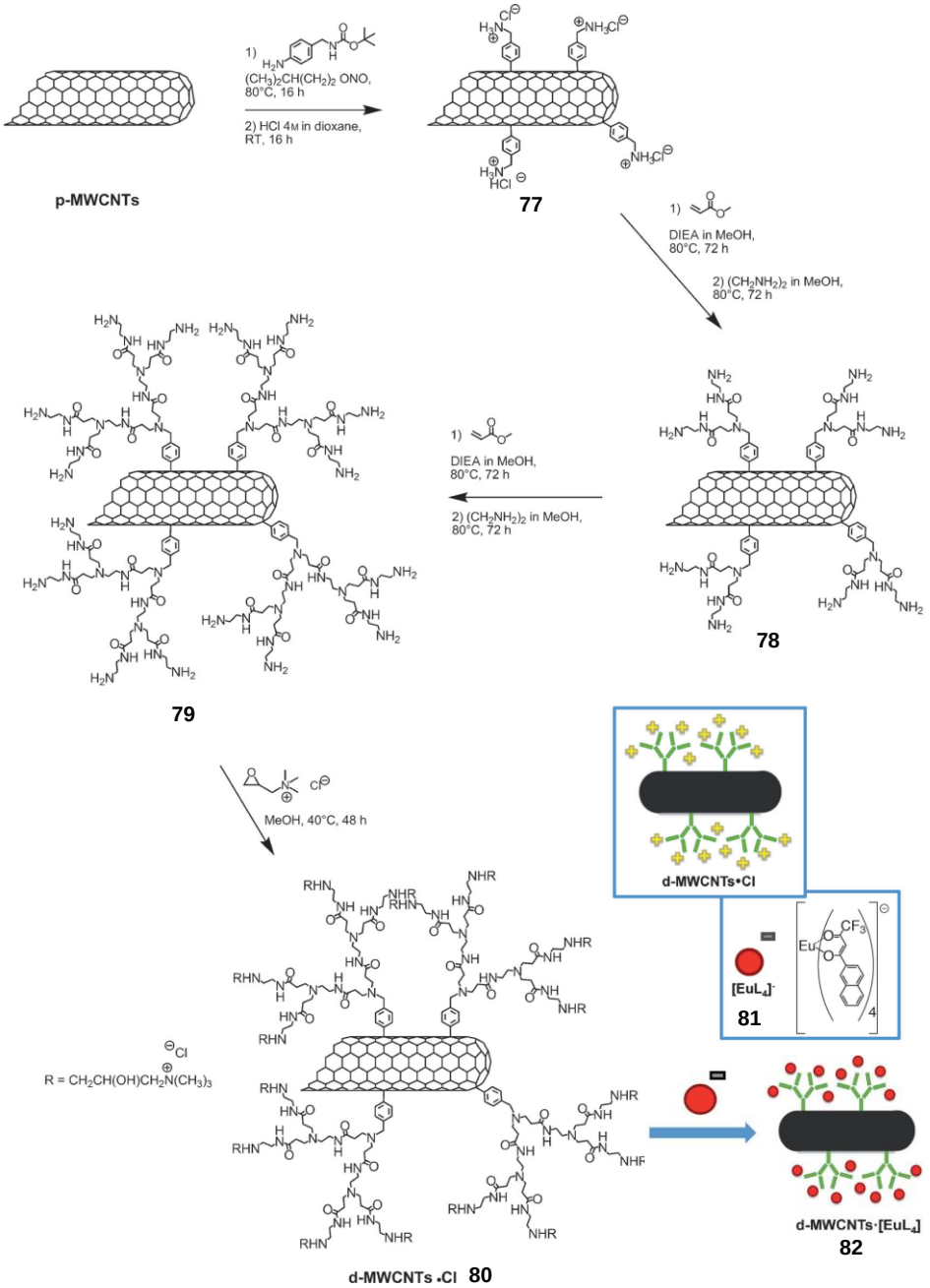

Scheme 23. Synthetic pathway towards d-MWCNTs·[EuL_4] **82**.

Carbon nanohorns (CNHs) represent a rather unexplored carbon allotrope, within the family of fullerenes and nanotubes. CNHs are produced in high yields upon laser ablation of graphite and are completely insoluble in all organic solvents However, CNHs have the advantage of being completely free from metal nanoparticles and carbonaceous and other amorphous material impurities. They are typically composed of a series tubes of about 2–5 nm in diameter and 30 to 50 nm long, closed by a cone at one extremity and associated with each other to give rise to round-shaped aggregates of 100 nm in diameter.

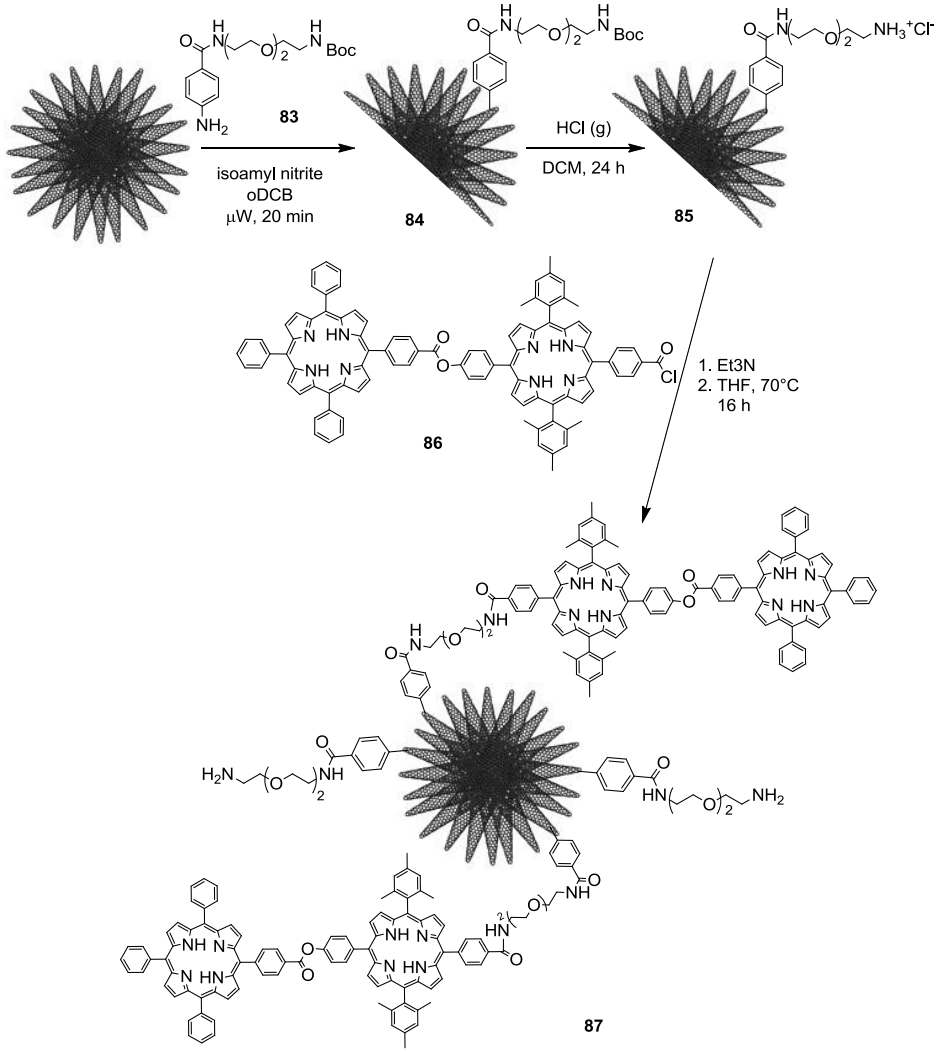

Scheme 24. Preparation of CNH−$(H_2P)_2$ hybrid **87**.

In order to build devices constructed of CNHs on substrates, fine dispersions must be obtained. Thus, it is essential to chemically functionalize and solubilize CNHs. Recently, CNHs have been successfully modified through a fast microwave assisted Tour reaction (Scheme 24).[18] Aniline **83** reacted with isoamyl nitrite to form the corresponding aryl diazonium salt which is linked to the CNHs. Then deprotection of Boc groups led to the free amino functionalities which in turn reacted with the acyl chloride of the dimeric porphyrin $(H_2P)_2$ **86** to afford the final hybrid **87**. TGA analysis showed that although **86** has been incorporated on the CNHs surface, only the half of the amino groups reacted. ATR-IR confirmed the presence of the features of both CNHs and porphyrin whilst Raman spectroscopy evidenced a slight increase in D-band, characteristic of the chemical saturation of CNHs double bonds.

On the other hand, the electrochemical characterization showed three one-electron reductions and a one-electron oxidation processes for the CNH-$(H_2P)_2$ hybrid **87**. The two reductions and the oxidation refer to the $(H_2P)_2$ unit, while the weak broad signal of the third reduction centered at -0.14 V refers to CNHs. Fluorescence and nanosecond transient absorption studies clearly demonstrated electron interaction between the two electroactive parts and the formation and decay of a charge-separated state of $CNH^{\bullet-}-(H_2P)_2^{\bullet+}$. Notably, the rate constant for charge separation in CNH−$(H_2P)_2$ hybrid **87** is larger than that for charge recombination by two orders making feasible to extract the separated charges, electrons and holes, by incorporating **87** into a photovoltaic cell (Fig. 11). Hence, a photoelectrochemical cell has been fabricated by electrophoretic deposition of **87** onto nanostructured SnO_2 films on an optically transparent electrode (OTE). The OTE/SnO_2/CNH−$(H_2P)_2$ electrode revealed prompt, stable, and reproducible photocurrent and photovoltage, with an incident photon-to-current conversion efficiency (IPCE) value as large as 9.6%, without the application of bias voltage. This was the highest IPCE observed for CNH-based hybrid two-compartment cells achieved thank to the high loading of the electron donor and its high molar absorptivity which enhanced and improved the photoinduced electron transfer efficiency in such hybrid materials.

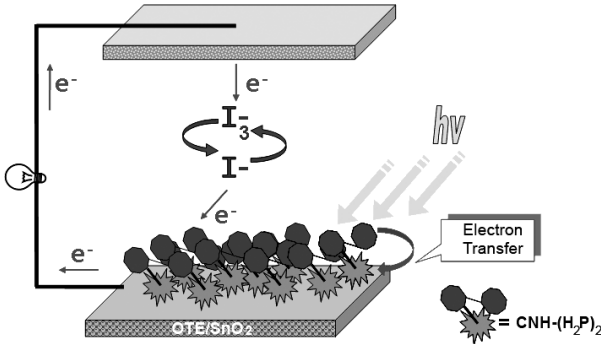

Fig. 11. Graphical representation of photoelectrochemical cell with OTE/SnO_2/CNH−$(H_2P)_2$ electrode. Reprinted with permission from ref. 18. © 2012 ACS.

Nanodiamonds, NDs, have recently received considerable attention due their favorable properties such as chemical inertness, biocompatibility, rather easy availability among others which make them as ideal materials for biomedical and electronic applications such as luminescence imaging, drug delivery, quantum engineering, surface coatings, seeding etc. For most of these fields a suitable surface termination and functionalization of the diamond materials are required. NDs have been functionalized with carbohydrates in order to explore their activity in the detection and agglutination of bacteria.[19]

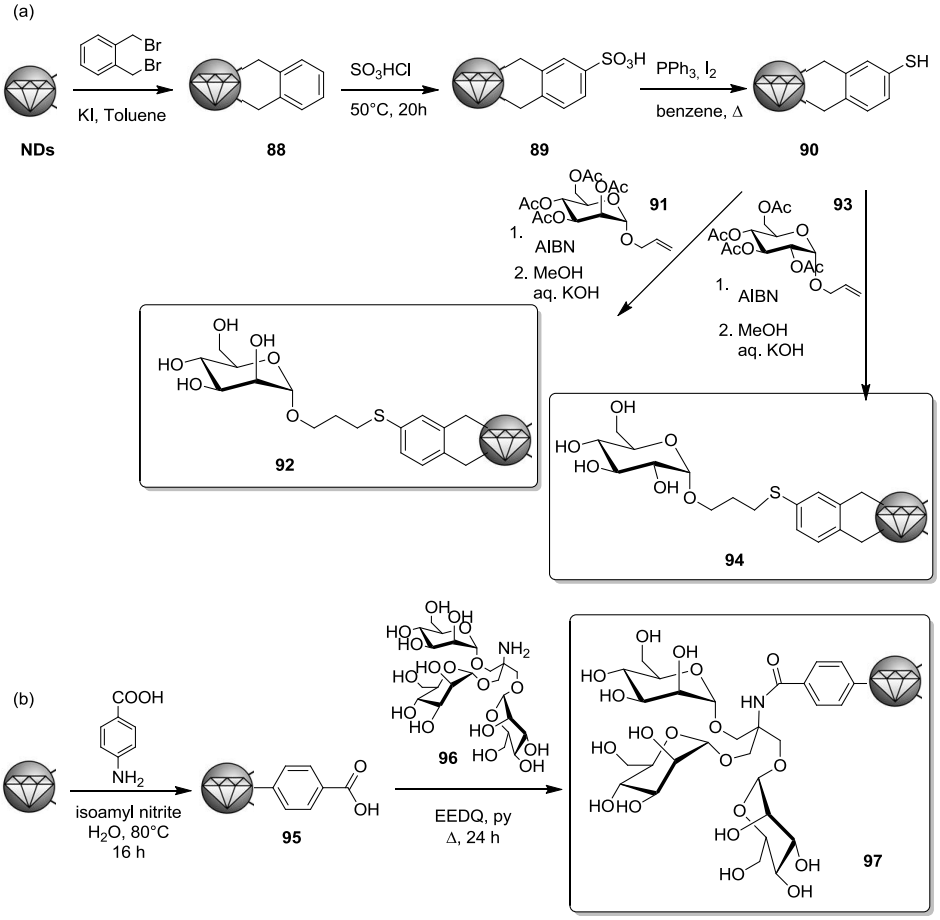

Scheme 25. Synthesis of NDs glycoconjugates **92**, **94** and **97**.

Two different synthetic strategies have been followed in order to prepare three glycol-nanodiamonds (Scheme 25). Firstly, a Diels–Alder cycloaddition on thermally annealed detonation NDs with in situ generated ortho-quinodimethane has been carried out to yield covalently arylated NDs (**88**) with surface loading of 0.14 mmol/g. After a classical aromatic sulfonation, one third of the sulfonic

acid groups was reduced by treatment with triphenylphosphine and iodine affording NDs **90**. The thiol functions allow the conjugation of the saccharide moieties on the diamond surface by "thiol–ene reaction" to the allyl aglycon of glycosides **91** and **93** giving rise after deprotection of acetyl groups to ND-conjugates **92** and **94**, respectively (Scheme 25a). In situ formed aryl diazonium salts are prone to functionalize also NDs-surface, in such a way nanodiamonds endowed with aryl carboxylic moieties **95** have been obtained with 0.19 mmol/g loading. Finally, the trivalent glycocluster **96** has been linked by peptide coupling employing the amino group at the focal point of the cluster mannoside with EEDQ as the coupling agent to afford the ND-glycoconjugate **97** (Scheme 25b). All the functionalized-NDs were characterized by means of FTIR, TGA and elementary analysis and Their full dispersion as isolated nanoparticles was shown by dynamic light scattering (DLS) and AFM measurements.

The carbohydrate decoration of ND conjugates **92**, **94** and **97** resembles parts of the eukaryotic glycocalyx and hence they can be regarded as mimetics of the host cells of bacteria. In this light, NDs-conjugates were applied in detection and agglutination of such pathogens.

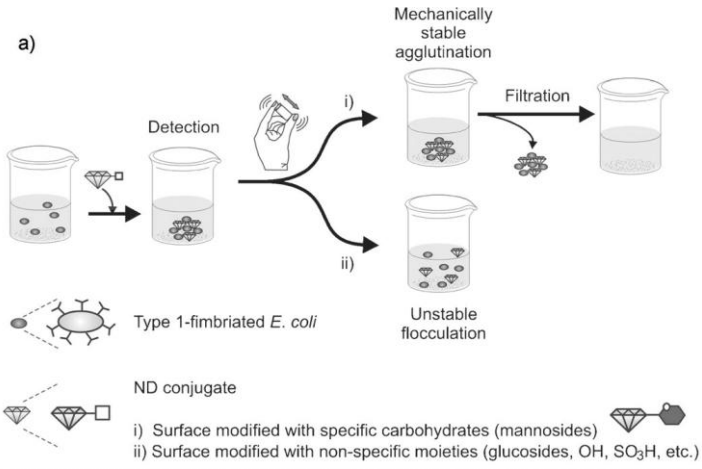

Fig. 12. Detection and removal of bacterial cells. Reprinted with permission from ref. 11. © 2012 John Wiley & Sons.

A suspension of fimbriated E. coli PKL1162 and six different ND samples (Fig.12) were diluted in water and mixed in test vials at ambient temperature. Equally, a suspension of non-fimbriated E. coli HB101 was mixed with serial dilutions of mannosylated NDs **92**. After a short incubation time of 5 min, precipitation was observed in all cases, even if the formed precipitates differed much in their visual characteristics as well as in their mechanical stability depending on the applied NDs. Whereas mannosylated NDs **92** and **94** formed well-structured crystal-like agglutinates with type 1 fimbriated E. coli, less compact flocculates were formed as a consequence of unspecific interactions of non-

mannosylated NDs. Moreover, mannosylated NDs samples **92** and **94** led to mechanically stable agglutinates in clear supernatant solution, which remained unaffected even after heavy manual shaking of the test vials. Interestingly, after filtration NDs can be recovered by reversing the agglutination using methyl α-D-mannopyranoside, a standard inhibitor of type 1 fimbriae-mediated bacterial adhesion.

References

1. Biboum, R. N.; Doungmene, F.; Keita, B.; de Oliveira, P.; Nadjo, L.; Lepoittevin, B.; Roger, P.; Brisset, F.; Mialane, P.; Dolbecq, A.; Mbomekalle, I. M.; Pichon, C.; Yin, P.; Liu, T.; Contant, R. *J. Mater. Chem.* **2012**, *22*, 319.
2. Wang, Y.; Zhou, S.; Kong, D.; Yang, H.; Chai, W.; Kortz U.; Wu, L. *Dalton Trans.* **2012**, *41*, 10052.
3. Wang, Y.; Li, H.; Qi, W.; Yang, Y.; Yan, Y.; Li, B.; Wu, L. *J. Mater. Chem.* **2012**, *22*, 9181.
4. Carraro,M.; Fiorani, G.; Mognon, L.; Caneva, F.; Gardan, M.; Maccato, C.; Bonchio, M. *Chem. Eur. J.* **2012**, *18*, 13195.
5. Deng, H.; Grunder, S.; Cordova, K. E.; Valente, C.; Furukawa, H.; Hmadeh, M.; Gándara, F.; Whalley, A. C. Liu, Z.; Asahina, S.; Kazumori, H.; O'Keeffe, M.; Terasaki, O.; Stoddart, J. F.; Yaghi, O. M. *Science* **2012**, *336*, 1018.
6. Kong, G.-Q.; Ou, S.; Zou, C.; Wu, C.-D. *J. Am. Chem. Soc.* **2012**, *134*, 19851.
7. Zhu, W.; He, C.; Wu, P.; Wu, X.; Duan, C. *Dalton Trans.* **2012**, *41*, 3072.
8. Jing, X.; He, C.; Dong, D.; Yang, L.; Duan, C. *Angew. Chem. Int. Ed.* **2012**, *51*, 10127.
9. Bortolini, O.; Caciolli, L.; Cavazzini, A.; Costa, V.; Greco, R.; Massi, A.; Pasti, L. *Green Chem.* **2012**, *14*, 992.
10. Xiao, W.; Jin, R.; Cheng, T.; Xia, D.; Yao, H.; Gao, F.; Deng, B.; Liu, G. *Chem. Commun.* **2012**, *48*, 11898.
11. Xu, Y.; Cheng, T.; Long, J.; Liu, K.; Qian, Q.; Gao, F.; Liu, G.; Li, H. *Adv. Synth. Catal.* **2012**, *354*, 3250.
12. Agrigento, P.; Beier, M. J.; Knijnenburg, J. T. N.; Baiker, A.; Gruttadauria, M. *J. Mater. Chem.* **2012**, *41*, 20728.
13. Riente, P.; Yadav, J.; Pericàs, M. A. *Org. Lett.* **2012**, *14*, 3668.
14. Hu, A.; Liu, S.; Lin, W. *RSC Adv.* **2012**, *2*, 2576.
15. Li, Y.; Li, G.; Wang, X.; Zhu, Z. Ma, H.; Zhang, T.; Jin, J. *Chem. Commun.* **2012**, *48*, 8222.
16. Kim, Y. S.; Cha, A.; Shin, J. Y.; Jeon, K. J.; Shim, J. H.; Lee, C.; Lee, S. *Chem. Commun*. **2012**, *48*, 8940.

17. Maggini, L.; Toma, F. M.; Feruglio, L.; Malicka, J. M.; Da Ros, T.; Armaroli, N.; Prato, M.; Bonifazi, D. *Chem. Eur. J.* **2012**, *18*, 5889.
18. Pagona, G.; Zervaki, G. E.; Sandanayaka, A. S. D.; Ito, O.; Charalambidis, G.; Hasobe, T.; Coutsolelos, A. G.; Tagmatarchis, N. *J. Phys. Chem. C* **2012**, *116*, 9439.
19. Hartmann, M.; Betz, P.; Sun, Y.; Gorb, S. N.; Lindhorst, T. K.; Krueger, A. *Chem. Eur. J.* **2012**, *18*, 6485.

Further readings

Chemistry of materials

1. Gómez-Romero, P.; Sanchez, C. editors in *"Functional Hybrid Materials*", Wiley-VCH, Weinheim, 2004**.**
2. Fahlman, B. H. in "Materials Chemistry", Springer, Dordrecht, 2007.
3. Atwood, J. L.; Steed, J. W. editors in "*Organic Nanostructures*", Wiley-VCH, Weinheim, 2008**.**

Polyoxometalates

4. Yamase, T.; Pope, M. T. editors in "*Polyoxometalate Chemistry for Nano-Composite Design*", Kluwer Academic, New York.
5. Proust, A.; Matt, B.; Villanneau, R.; Guillemot, G.; Gouzerh, P.; Izzet, G. *Chem. Soc. Rev.* **2012**, *41*, 7605.
6. Miras, H. N.; Yan, J.; Long, D.-L.; Cronin, L. *Chem. Soc. Rev.* **2012**, *41*, 7403.

Metal-Organic Frameworks

7. MacGillivray, L. R. editor "*Metal-Organic Frameworks: Design and Applications*", John Wiley & Sons, Hoboken, 2010.
8. James, S. L.; *Chem. Soc. Rev.* **2003**, *30*, 276.
9. Yaghi, O. M.; O'Keeffe, M.; Ockwig, N. W.; Chae, H. K.; Eddaoudi, M.; Kim, J. *Nature* **2003**, *243*, 705.

Amorphous and Mesostructured Hybrid Silica

10. Koch, C. C. editor in "*Nanostructured Materials: Processing, Properties, and Applications*" 2nd ed., William Andrew, Norwich, USA, 2007.
11. Jutzi, P.; Schubert, U. editors in "*Silicon Chemistry",* Wiley-VCH, Weinheim 2003.
12. Bergna, H. E.; Roberts, W. O. editors in "*Colloidal Silica: Fundamentals and Applications*", CRC, Boca Raton, 2006.

Magnetic Nanoparticles

13. Lu, A.-H.; Salabas, E. L.; Schüth, F. *Angew. Chem. Int. Ed.* **2007**, *46*, 1222.
14. Hyeon, T. *Chem. Commun.* **2003**, 927.
15. Frey, N. A.; Peng, S.; Cheng, K.; Sun, S. *Chem. Soc. Rev.* **2009**, *38*, 2532.

Carbon Nanoforms

16. Akasaka, T.; Wudl, F. editors in "*Chemistry of Nanocarbons*", John Wiley, Chichester, 2010.
17. Delgado, J. L.; Herranz, M. A.; Martín, N. *J. Mater. Chem.* **2008**, *18*, 1417.
18. Tasis, D.; Tagmatarchis, N.; Bianco, A.; Prato, M. *Chem. Rev.* **2006**, *106*, 1105.
19. Mochalin, V. N.; Shenderova, O.; Ho, D.; Gogotsi, Y. *Nat. Nanotech.* **2012**, *7*, 11.